J. Fluid Mech. (1978), *vol.* 87, *part* 3, *pp.* 533–560
Printed in Great Britain

The dynamics of carangiform swimming motions

By T. KAMBE

Department of Physics, University of Tokyo, Japan†

(Received 26 July 1977)

An investigation based on the elongated-body theory of Lighthill (1960, 1970) and Wu (1971) is made of the carangiform swimming motions of fish, a mode of propulsion in which the amplitude of body undulation becomes significant only in the posterior half, or even third, of the length of the fish and the anterior part is relatively inflexible. For typical slender fish performing undulatory swimming motions, three hydrodynamic features are taken into account: (*a*) the resistance to the lateral undulatory motions as well as longitudinal (tangential) frictional resistance, (*b*) the forces of interaction with the water associated with its inertial (virtual-mass) response to the lateral motions of the fish and (*c*) the reaction forces due to the vortex sheets shed from sharp trailing edges to the rear of the section of maximum span (depth), where a great variety of fins are generally found.

The active tail oscillations give rise to oscillatory side forces, to which the remainder of the body responds passively. These passive yawing motions are studied to find their amplitude, the yawing axis and any associated energy dissipation. The contribution of each of the above three forces is examined and the effects of the oscillation frequency, a slenderness parameter δ of the body, and the shape of the transverse cross-sections are considered.

The present theory is further applied to predict the turning movement when the fish changes direction, the way in which the above forces act during this process being investigated. A small perturbation analysis relative to a uniform rectilinear motion not only reveals whether or not the motion is dynamically stable, but also leads to a full description of the motion that follows a given initial perturbation. For finite perturbations a numerical method is adopted to find the time development of both the direction of motion relative to the direction of the initial uniform motion and the ratio of the kinetic energy of the body to the initial kinetic energy for different magnitudes I_0 of the initial impulsive perturbation in the transverse direction. The final angle of turn is obtained in terms of I_0 for different values of δ. The loss of kinetic energy during the turn divided by the initial kinetic energy is found to be very small for a small angle of turn.

Detailed analyses are made for rigid fish models in which the distribution of depth (or span) along the body length is quadratic with a maximum at the centre. Agreement of the present analyses with observations is fairly good at least qualitatively and some quantitative estimates are made of the side forces, both oscillatory and impulsive, exerted on the body by the tail. It is found that the vortex sheets shed from trailing edges increase the energy loss due to the yawing oscillations, in addition to the resistive dissipation, but contribute to the directional stability of rectilinear motion.

† Present address: Department of Applied Science, Faculty of Engineering, Kyushu University, Fukuoka 812, Japan.

1. Introduction

The swimming modes of fishes may be divided into two main classes, anguilliform and carangiform, with a few exceptions (Lighthill 1969). In the anguilliform mode of swimming the whole body is flexible and the amplitude of the propulsive wave, which travels from head to tail, is significant all along the fish's length, although it increases towards the tail. In carangiform swimming, by contrast, the amplitude of undulation becomes significant only in the posterior half, or even third, of the length of the fish and the anterior part is relatively inflexible. The carangiform mode is found in fishes in classes of advanced orders which are strong, active swimmers, achieving high hydromechanical efficiency (Lighthill 1970). They propel themselves primarily by active tail oscillations, to which the remainder of the body responds passively.

According to Lighthill (1970), two characteristics of the morphology of carangiform swimmers have the function of reducing these recoil motions. A long anterior region of high depth is important because it responds to the side forces associated with the thrusting oscillatory movement as if its inertia were augmented by the virtual mass (also called the added mass) of water associated with its lateral motion. The yawing response is diminished in the presence of a large moment of inertia. Equally important is the presence of a region of greatly reduced depth (the caudal peduncle) between the actively thrusting caudal fin and the passively responding anterior portion.

A fish-like body is typically slender in the spanwise (depth) direction compared with its length l and of yet smaller thickness in the lateral direction. The slenderness parameter δ, defined as s_m/l (s_m being the maximum depth), is about 0·4–0·2 if the body depth is measured with the dorsal and ventral fins extended (Wu 1971). In general the transverse cross-sections of the body are more or less elliptical, with a ratio σ of the minor to the major axis of around 0·6 for some slightly compressed species, and have rather rounded edges anterior to the section of widest span, becoming lenticular in shape in the posterior part of body, where there are a great variety of dorsal, ventral and other fins, followed by a tail-base neck just ahead of the caudal fin.

Lighthill (1960) investigated the swimming of a slender fish performing movements transverse to its direction of motion. From 'elongated-body' theory, he obtained the propulsive thrust produced by the movement and its time rate of working. There exist some slender fishes of the 'ribbon-fin' type whose transverse cross-section to the rear of the section of maximum span is of a lenticular shape with sharp edges, like those of spiny fins, from which an oscillating vortex sheet is shed. An important extension of Lighthill's (1960) theory was made by Wu (1971) to determine the effect of the vortex-sheet shedding on the swimming performance of a fish with ribbon fins with a gradual change in slope. The leading edges were assumed to be sufficiently rounded to prevent flow separation. The Kutta condition was assumed to hold at the sharp trailing edges, from which a vortex sheet was shed in unsteady motion. Lighthill (1970) examined, by contrast, fins with unswept straight edges, assuming that the body sections behind the fins were smooth and did not shed any further vorticity. A general slender-body theory capable of embracing a wide variety of fin configurations was developed by Newman & Wu (1973), and included interactions between the body thickness and the trailing vortex sheets.

The caudal fin, which is linked rather flexibly to the main body, generates thrust and side forces through lateral oscillations of large amplitude. These in turn are

produced by oscillatory side forces exerted by the body musculature on the caudal fin. To every action there is an equal and opposite reaction so the anterior part of the body is also subjected to oscillatory side forces. Any large yawing motions with which the anterior part of the body responds to such oscillatory side forces greatly increase the energy dissipation involved in swimming. As a complementary theory to the hydrodynamics of thrust generation by the caudal fin, Lighthill (1977) developed a new theory of recoil based on the philosophy of Lighthill (1970), viz. a reactive–resistive theory, and estimated the amplitude of the yawing motion and the associated energy dissipation.

In § 2 the equations of motion of the reactive–resistive theory, which is based on the 'elongated-body' theory (Lighthill 1970, 1977), are presented. The equations are extended to cover cases both with and without vortex-sheet shedding from the trailing edge, following Wu (1971), and further modified slightly to facilitate the analysis of turning in § 4. In § 3 the effects of both vortex-sheet shedding and normal drag forces on the recoil movements are studied and the associated energy dissipation is estimated. A refined numerical analysis using an iteration method is also presented.

A mathematical theory of the turning manoeuvre when a fish suddenly changes direction is presented in § 4. According to observations, directional control in fish is achieved in two ways (Gray 1968). When a fish is moving relatively slowly, paired fins such as the pectoral fins are used to change its direction either passively, by altering their angle of incidence, or actively, by propelling one side faster than the other. But when a fish is swimming rapidly the fins are usually held close to the sides of the body, and yet the fish can carry out very rapid changes in the direction of motion. A theoretical and quantitative approach to turning motion of the latter kind from a hydrodynamical point of view was first made by Weihs (1972), on the basis of films taken by Sir James Gray, parts of which appear in Gray (1933, 1968). Recently McCutchen visualized fish wakes by a shadowgraph method, a single frame from a movie film taken by a 3·15 cm Zebra Danio camera being shown in McCutchen (1976). This indicates that two vortex blobs (probably with the structure of vortex rings) are shed successively by the tail during the turn, the first (smaller) one being shed on the side corresponding to the direction of turn and the second (larger) one on the opposite side but almost to the rear with respect to the new direction of motion. A vortex ring carries a certain amount of momentum determined by its size and vorticity distribution. Accordingly, the shedding of a vortex ring gives rise to a reaction force on the body of the fish. This force is represented by an impulsive force in the mathematical model of turning in § 4. The theory also takes into account drag forces and also reactive forces associated with the shedding of vortex sheets from sharp edges, both of which provide the centripetal force necessary for the turn. This manoeuvre in water is in striking contrast to the 'banked turn' of flying animals or aeroplanes, whose inclined position supplies the lateral component of the lift needed for the turn.

The investigation of infinitesimal perturbations to a uniform rectilinear motion in § 4 not only helps to decide whether or not the motion is dynamically stable, but also leads to a full description of the motion that follows a given initial perturbation in a hypothetical dragless fluid.

The present study is intended to give a mathematical formulation and solution which will be accurate enough to describe and predict the principal mechanism of both the passive response of the anterior part of carangiform swimmers and the

turning manoeuvre of the fish, perhaps not with complete precision but at least avoiding serious physical errors. The present analyses are based on the following basic ideas, theories and assumptions.

(i) The elongated-body theory (unsteady slender-body theory) developed by Lighthill (1960, 1970) and Wu (1971) is applied. In a frame of reference moving with the fish's mean speed U, the fish is making undulatory movements in order to remain in the same average position in a stream whose undisturbed velocity is U, directed along the x axis. The cross-section of the fish at a distance x from the front is supposed to be displaced by an amount $h(x,t)$ in the direction z normal to the x axis. Following Lighthill (1970), we use W for the lateral velocity $\partial h/\partial t$ of the cross-section at x and also

$$w = \partial h/\partial t + U\partial h/\partial x \tag{1.1}$$

for the velocity of lateral pushing of a vertical slice of water (perpendicular to the fish's longitudinal axis) by the successive cross-sections past which it sweeps with velocity U. The lateral pushing with velocity $w\mathbf{n}$ ($\mathbf{n}$ being a unit vector perpendicular to the fish's backbone) gives rise to lateral momentum $m_a w\mathbf{n}$ per unit length in the water slice, where m_a is the added mass of the water per unit length of the fish. Lighthill (1970) gives a full discussion, taking

$$m_a = \alpha_2 \rho s^2, \tag{1.2}$$

where ρ is the water density and $s(x)$ the depth of the cross-section, in which case $\alpha_2/\frac{1}{4}\pi$ is a non-dimensional parameter of order unity which is exactly unity for an elliptic cross-section of any eccentricity. The force in the $\mathbf{n}$ direction which the fish exerted on a water slice, per unit distance in the x direction, must equal the rate of change of the $\mathbf{n}$ component of momentum of the water slice as it sweeps past the undulating fish at velocity U. This reactive force is thus

$$G = (\partial/\partial t + U\partial/\partial x)\, m_a(x)\, w(x,t), \tag{1.3}$$

for a smoothly shaped section with rounded edges. On the other hand, Wu's (1971) theory takes into account the vortex-sheet shedding at the body sections with sharp trailing edges to the rear of the section of maximum span. The effect of shedding a vortex sheet is equivalent to treating m_a as constant when calculating the change in the cross-flow momentum. Thus the reactive force in the $\mathbf{n}$ direction is

$$G = m_a\left(\frac{\partial}{\partial t} + U\frac{\partial}{\partial x}\right) w = \left(\frac{\partial}{\partial t} + U\frac{\partial}{\partial x}\right) m_a w - Uw\frac{d}{dx} m_a \tag{1.4}$$

in the posterior sections with sharp edges, from which a vortex sheet is shed into the wake. It is also suggested by Wu (1971) that this effect, represented by the second term of (1.4), may possibly enhance the thrust production. Comparison of (1.3) and (1.4) enables one to write the reactive force G in the composite form

$$G = (\partial/\partial t + U\partial/\partial x)\, m_a w - \epsilon_1 U w m_a', \tag{1.5}$$

where $m_a' = dm_a/dx$, and $\epsilon_1 = 0$ at sections with rounded edges and $\epsilon_1 = 1$ at sections with sharp edges. In many slender fishes, however, one observes that the body sections behind the dorsal fin are also smoothly shaped and do not shed any vorticity, making $\epsilon_1 = 0$.

(ii) In order to investigate the effect of the vortex-sheet shedding on the swimming performance, we examine two cases:

(*A*) $\epsilon_1 = 0$ for the sections anterior to the section of maximum span, and $\epsilon_1 = 1$ for the sections posterior to that section;

(*B*) $\epsilon_1 = 0$ all along the body length.

(iii) When pushing a slice of water, a body section experiences hydrodynamic resistance in addition to the reactive force mentioned in (i). This resistive force may increase the energy dissipation involved in swimming when the anterior part of the body responds passively to the oscillatory lateral forces. Here we consider an approximate relation between the resistive force (per unit length) and the lateral motions with velocity w perpendicular to the backbone. Fish cross-sections of depth s and much smaller width (in the direction of w) are likely to give almost as much resistance as a flat plate of the same depth s. Such a plate moving perpendicular to itself at a steady velocity experiences a resistance $\frac{1}{2}\rho w^2 s C_n$ per unit length. Following Lighthill (1977), the resistance formula

$$D_n \mathbf{n} = -\tfrac{1}{2}\rho C_n s|w|w\mathbf{n} \tag{1.6}$$

per unit length is adopted here to describe the resistance to the normal motion $w\mathbf{n}$. The drag coefficient $C_n = 2$ will give an upper limit (Flachsbart 1935) by means of which the maximum possible importance of resistive forces relative to reactive forces can be estimated. We may assume a tangential frictional resistance of the form

$$D_t = \tfrac{1}{2}\rho C_f s u_t^2 \tag{1.7}$$

per unit length, where u_t is the tangential velocity of the body surface relative to the water.

(iv) In order to investigate the dynamical movements of the anterior part of the body of a slender fish performing carangiform motion, the relatively inflexible anterior portion is represented by a rigid fish-like model of depth

$$s(\xi) = s_m[1 - (\xi/a)^2], \quad -a \leqslant \xi \leqslant a, \tag{1.8}$$

where s_m is the maximum depth, $2a$ is the length of the body while ξ is the co-ordinate along the length and is fixed relative to the fish with origin at its midpoint. Large amplitude lateral movement of the caudal fin produces a reactive force, to which the anterior part responds passively. Thus the tail-less model is considered to be subjected to an unsteady force $\mathbf{F}(t)$ acting at the posterior end, in addition to the reactive forces (i) and the resistive forces (iii). It is thought that a flexible link at the peduncle reconciles the two different motions. As shown by the analysis of Chopra & Kambe (1977) and interpreted physically by Lighthill (1977), the driving force is fairly closely in phase with the fin's own lateral velocity for high frequency tail oscillations in lunate-tailed animals.

(v) The body's mass m_b per unit length may be written as

$$m_b = \alpha_1 \rho s^2, \tag{1.9}$$

where α_1 is a numerical constant. If the cross-section is an ellipse for which the ratio of the minor axis to the major is σ, one has

$$\alpha_1 = \tfrac{1}{4}\pi\sigma, \quad \alpha_2 = \tfrac{1}{4}\pi; \quad \text{thus} \quad \alpha_1/\alpha_2 = \sigma. \tag{1.10a, b, c}$$

We assume that α_1 is independent of ξ, i.e. the cross-sections are similar along the body length. Strictly speaking, this may contradict case (ii$A$), in which the value of ϵ_1 is not constant along the body length. It is thought, however, that any longitudinal asymmetry of the cross-section is represented by the second term of (1.5).

In the following we assume the relations (1.10b, c) generally whether or not the cross-sections are elliptical, and also write

$$\alpha_0 = \alpha_1 + \alpha_2, \quad \gamma_1 = \frac{\alpha_1}{\alpha_0} = \frac{\sigma}{1+\sigma}, \quad \gamma_2 = \frac{\alpha_2}{\alpha_0} = 1 - \gamma_1, \qquad (1.11a, b, c)$$

α_0 being given by $(1+\sigma)\alpha_2$ or $\frac{1}{4}(1+\sigma)\pi$.

Watanabe & Kimura (1977) made a biomechanical study of carp to fabricate a self-propelled mechanical fish. Measurement of the cross-sections of the body of a sample fish (Watanabe & Kimura, private communication) shows that the value of σ for its nearly elliptical cross-sections, excluding fins, varies from about 1 near the nose to 0·5 or a little less near the peduncle with an average value 0·60. In front sections anterior to that of maximum depth σ is larger than 0·6 while in the posterior sections it is about 0·5.

2. Equations of motion in reactive–resistive theory

The inflexible anterior portion is subjected to the reactive forces (i), the resistive forces (iii) and the force $\mathbf{F}(t)$ at $\xi = a$ given in (iv). In order to describe the motions generally, we choose a Cartesian co-ordinate system (X, Y, Z) fixed in space in which the fluid is at rest at infinity. The position vector of the centre of mass of the body is written as a function of time t: $\mathbf{X}_0(t) = (X_0(t), Y_0(t), Z_0(t))$. It is supposed that the axis of the body always lies in the plane $Z = 0$. This is made possible by assuming that the Z components of the force acting on the fish balance at each cross-section, assumed symmetric with respect to the plane $Z = 0$, and therefore the resultant of the forces has only X and Y components. Thus the Z components of vectors are ignored in the following analysis. The depth s of a cross-section is used as the size in the Z direction. The angle between the X axis and the body axis is denoted by θ (figure 1). It is convenient to define a tangential unit vector $\mathbf{t}$, a normal unit vector $\mathbf{n}$ and a unit vector $\mathbf{e}_X$ in the $-X$ direction by

$$\mathbf{t} = (\cos\theta, \sin\theta), \quad \mathbf{n} = (-\sin\theta, \cos\theta), \quad \mathbf{e}_X = (-1, 0), \qquad (2.1a, b, c)$$

where $\mathbf{t}$ points from the nose to the tail and turning $\mathbf{t}$ anticlockwise through 90° yields $\mathbf{n}$. Thus in terms of ξ (a Lagrangian co-ordinate along the body axis) the position $\mathbf{X}$ of a cross-section is written as

$$\mathbf{X} = (X, Y) = \mathbf{X}_0 + \xi\mathbf{t} \quad (-a \leqslant \xi \leqslant a), \qquad (2.2)$$

the nose lying at $\xi = -a$ and the posterior end at $\xi = a$. The velocity $\mathbf{V}$ and acceleration $\mathbf{A}$ of a section with a fixed ξ are

$$\mathbf{V} = \dot{\mathbf{X}} = \mathbf{V}_0 + \xi\dot{\theta}\mathbf{n}, \qquad (2.3a)$$

$$\mathbf{V}_0 = (V_{0X}, V_{0Y}) = \dot{\mathbf{X}}_0, \quad V_{0n} = \mathbf{V}_0 \cdot \mathbf{n}, \quad V_{0t} = \mathbf{V}_0 \cdot \mathbf{t}, \qquad (2.3b, c, d)$$

$$\mathbf{A} = \dot{\mathbf{V}} = \mathbf{A}_0 + \xi\ddot{\theta}\mathbf{n} - \xi\dot{\theta}^2\mathbf{t}, \qquad (2.4a)$$

$$\mathbf{A}_0 = \dot{\mathbf{V}}_0, \quad A_{0n} = \mathbf{A}_0 \cdot \mathbf{n}, \quad A_{0t} = \mathbf{A}_0 \cdot \mathbf{n}, \qquad (2.4b, c, d)$$

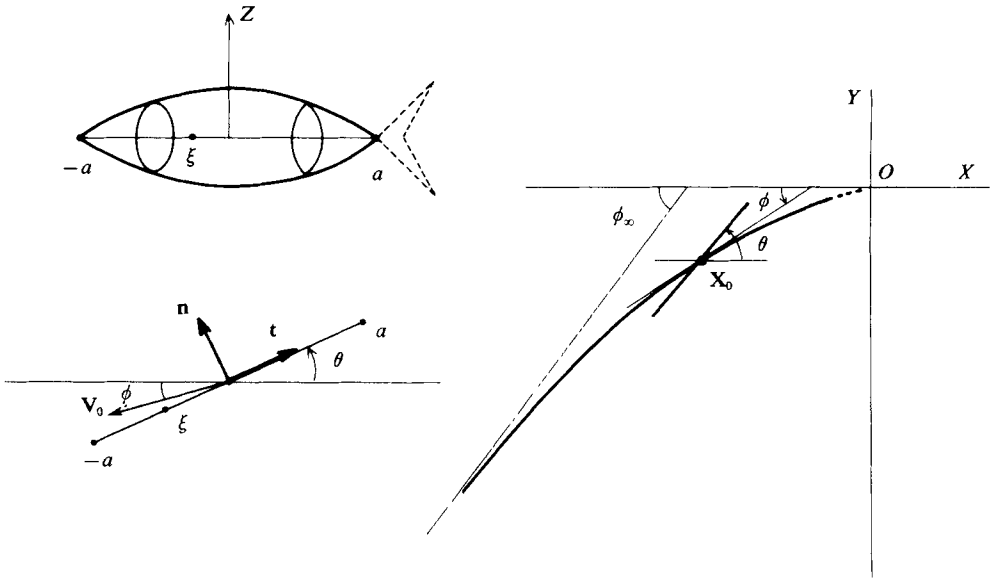

FIGURE 1. Definition sketch of the co-ordinate system.

where a dot denotes differentiation with respect to time t and the relations $\dot{\mathbf{t}} = \dot{\theta}\mathbf{n}$ and $\dot{\mathbf{n}} = -\dot{\theta}\mathbf{t}$ have been used. It should be noted that, although the motion of the centre of mass considered here is not necessarily rectilinear, the angle $\theta - \phi$ between the body axis and the direction of motion of the centre of mass is assumed to be small, where

$$\phi = \cos^{-1}[(\mathbf{V}_0 . \mathbf{e}_X)/|\mathbf{V}_0|], \tag{2.5}$$

the angle between the x axis and the direction of motion of the centre of mass, so that the perturbation theory of the swimming of a slender fish mentioned in (i) in § 1 is still applicable. Thus the lateral pushing velocity defined by (1.1) is given by the normal component V_n of the velocity of a section:

$$V_n = \mathbf{V} . \mathbf{n} = V_{0n} + \xi\dot{\theta} = \dot{\theta}(b + \xi), \tag{2.6}$$

where

$$b = V_{0n}/\dot{\theta}. \tag{2.7}$$

The velocity U of the free stream in the frame of reference fixed to the fish is given by minus the tangential component of the velocity of the centre of mass:

$$U = -\mathbf{V}_0 . \mathbf{t}. \tag{2.8}$$

Therefore the force G in the $\mathbf{n}$ direction, defined by (1.5), which the fish exerts on the fluid can be written as

$$G = (\partial/\partial t + U\,\partial/\partial\xi)\, m_a V_n - \epsilon_1 U V_n m_a'. \tag{2.9}$$

The resistance (1.6) to the normal motion and the tangential frictional resistance (1.7) can be expressed similarly and combined to give the total drag per unit length:

$$\mathbf{D} = D_n \mathbf{n} + D_t \mathbf{t}, \tag{2.10}$$

where

$$D_n = -\tfrac{1}{2}\rho C_n s |V_n| V_n, \quad D_t = \tfrac{1}{2}\rho C_f s U^2. \tag{2.11 a, b}$$

The rigid fish model (iv), which is subjected to the three forces $-G(\xi)\mathbf{n}$, $\mathbf{D}(\xi)$ and $\mathbf{F}(t)$ at $\xi = a$, makes a response in which the lateral velocity has the form (2.6) and which satisfies the equations of momentum and angular momentum. The equation describing the conservation of momentum takes the form

$$\int_{-a}^{a} m_b \mathbf{A}\, d\xi = -\mathbf{n}\int_{-a}^{a} G\, d\xi + \int_{-a}^{a} \mathbf{D}\, d\xi + \mathbf{F}. \tag{2.12}$$

Similarly the equation of angular momentum about $\xi = 0$ is

$$\int_{-a}^{a} m_b A_n \xi\, d\xi = -\int_{-a}^{a} G\xi\, d\xi + \int_{-a}^{a} D_n \xi\, d\xi + F_n a, \tag{2.13}$$

where $A_n = \mathbf{A}.\mathbf{n}$ and $F_n = \mathbf{F}.\mathbf{n}$. Hereafter we assume longitudinal symmetry of the fish's mass distribution, i.e. a symmetric distribution of depth s along the length such that

$$s(-\xi) = s(\xi) \tag{2.14a}$$

and hence

$$m_b(-\xi) = m_b(\xi), \quad m_a(-\xi) = m_a(\xi) \tag{2.14b, c}$$

by (1.2) and (1.9). Then the term on the left-hand side of (2.12), with $\mathbf{A}$ given by (2.4a), becomes

$$\int_{-a}^{a} m_b [\mathbf{A}_0 + \xi(\ddot{\theta}\mathbf{n} - \dot{\theta}^2 \mathbf{t})]\, d\xi = M_b \mathbf{A}_0, \tag{2.15}$$

where

$$M_b = \int_{-a}^{a} m_b\, d\xi = \alpha_1 \rho K_0, \tag{2.16}$$

$$K_0 = \int_{-a}^{a} s^2\, d\xi, \tag{2.17}$$

M_b being the total body mass. Likewise the first term on the right-hand side of (2.12) (the inertial response of the water) can be written as

$$\int_{-a}^{a} G\, d\xi = \int_{-a}^{a} \left(\frac{\partial}{\partial t} + U\frac{\partial}{\partial \xi}\right) m_a V_n\, d\xi - \epsilon_1 U \int_0^a V_n m_a'\, d\xi \tag{2.18a}$$

$$= M_a \dot{V}_{0n} + \epsilon\Phi, \tag{2.18b}$$

where

$$M_a = \int_{-a}^{a} m_a\, d\xi = \alpha_2 \rho K_0, \tag{2.19}$$

$$\dot{V}_{0n} = d(\mathbf{V}_0.\mathbf{n})/dt = \dot{\mathbf{V}}_0.\mathbf{n} + U\dot{\theta}, \tag{2.20}$$

$$\Phi = U[m_a V_n]_{-a}^{a} - U\int_0^a V_n \frac{dm_a}{d\xi}\, d\xi \tag{2.21a}$$

$$= U m_a(0) V_{0n} + U\dot{\theta}\int_0^a m_a\, d\xi, \quad (m_a(-a) = 0), \tag{2.21b}$$

$$\epsilon = \begin{cases} 1 & \text{in case } A, \\ 0 & \text{in case } B, \end{cases}$$

M_a being the total added mass and $[f]_{x_1}^{x_2}$ denoting $f(x_2) - f(x_1)$. The function Φ represents the rate of transfer of lateral momentum to the water in the form of vortex sheets. As for the second term of (2.21a), which comes from the second integral in (2.18a),

the reason is evident. The first term $U[m_a V_n]_{-a}^{a}$, which arises from the second term in the first integral in (2.18a) and is given a full mechanical interpretation by Lighthill (1970), is associated with the rate of shedding of lateral momentum $m_a(a)\,V_n(a)$ per unit length into the wake from the trailing edge $\xi = a$ in the case $m_a(-a) = 0$, which is generally true for slender fish. For this reason the first term is included in Φ. This term, however, gives no contribution to the model (1.8) since $m_a(\pm a) = 0$.

Hence, by using (2.15) and (2.18b), the momentum equation (2.12) becomes

$$M_b \mathbf{A}_0 + (M_a \dot{V}_{0n} + \epsilon\Phi)\,\mathbf{n} = D_n^* \mathbf{n} + D_t^* \mathbf{t} + \mathbf{F}, \tag{2.22}$$

where

$$D_n^* = \int_{-a}^{a} D_n\,d\xi = -\frac{\rho}{2} C_n \int_{-a}^{a} s|V_n|V_n\,d\xi, \tag{2.23a}$$

$$D_t^* = \int_{-a}^{a} D_t\,d\xi. \tag{2.23b}$$

In almost the same way the angular momentum equation (2.13) reduces to

$$(I_b + I_a)\,\ddot{\theta} - M_a U V_{0n} + \epsilon\Psi = Q^* + F_n a, \tag{2.24}$$

where

$$I_b = \int_{-a}^{a} m_b \xi^2\,d\xi = \alpha_1 \rho K_2, \tag{2.25}$$

$$I_a = \int_{-a}^{a} m_a \xi^2\,d\xi = \alpha_2 \rho K_2, \tag{2.26}$$

$$K_2 = \int_{-a}^{a} \xi^2 s^2\,d\xi, \tag{2.27}$$

$$\begin{aligned}\Psi &= U[m_a \xi V_n]_{-a}^{a} - U\int_0^a \xi(V_{0n} + \xi\dot{\theta})\frac{dm_a}{d\xi}\,d\xi,\\ &= U[m_a \xi V_n]_{-a}^{a} - U[V_{0n}\xi m_a + \dot{\theta}\xi^2 m_a]_0^a + UV_{0n}\int_0^a m_a\,d\xi + U\dot{\theta}\int_0^a 2\xi m_a\,d\xi,\end{aligned} \tag{2.28}$$

$$Q^* = \int_{-a}^{a} D_n \xi\,d\xi = -\frac{\rho}{2} C_n \int_{-a}^{a} \xi s|V_n|V_n\,d\xi, \tag{2.29}$$

I_b and I_a being the moments of inertia of the body and the added mass about $\xi = 0$ respectively. The function Ψ represents the reaction from the shedding of vortex sheets, the reasoning being identical to that for Φ. Thus we find that the system of equations (2.22) and (2.24), together with the auxiliary definitions, (2.20), (2.21), (2.23), (2.28), (2.29) etc., constitutes a system of three simultaneous first-order differential equations for the three unknowns V_{0X}, V_{0Y} and $\dot{\theta}$.

For the following analysis, it is convenient to rewrite (2.22). Using (2.20) and rearranging, this can be written in the form

$$M_b \mathbf{A}_0 + M_a A_{0n}\,\mathbf{n} = H\mathbf{n} + D_t^* \mathbf{t} + \mathbf{F}, \tag{2.30}$$

where

$$H = -M_a U\dot{\theta} - \epsilon\Phi + D_n^*. \tag{2.31}$$

Then the $\mathbf{n}$ and $\mathbf{t}$ components of (2.30) are

$$M_0 A_{0n} = H + F_n, \quad M_b A_{0t} = D_t^* + F_t, \tag{2.32), (2.33}$$

where

$$M_0 = M_b + M_a = \alpha_0 \rho K_0. \tag{2.34}$$

This tells us that for lateral motions the system responds as if the inertia were the sum of the body mass M_b and the added mass M_a, under the influence of the force $H+F_n$, while for tangential motions the inertia includes only the body mass. The disappearance of the added mass for the longitudinal motions, which is much smaller than M_a, provides an estimate of the error involved in (2.30). Dividing (2.32) by M_0 and (2.33) by M_b, we obtain

$$\mathbf{A}_0 = A_{0n}\mathbf{n} + A_{0t}\mathbf{t} = M_0^{-1}(H+F_n)\,\mathbf{n} + M_b^{-1}(D_t^* + F_t)\,\mathbf{t}, \tag{2.35}$$

which is another form equivalent to (2.30).

The angular momentum equation (2.24) is written simply as

$$I_0\ddot{\theta} = R + F_n a, \tag{2.36}$$

where

$$R = M_a U V_{0n} - \epsilon\Psi + Q^*, \tag{2.37}$$

$$I_0 = I_b + I_a. \tag{2.38}$$

For the fish model (1.8) in (iv) in § 1, we have

$$\Phi = m_a(0)\,UV_{0n} + \tfrac{1}{2}M_a U\dot{\theta}, \tag{2.39}$$

$$\Psi = \tfrac{1}{2}M_a U V_{0n} + N_a U\dot{\theta}, \tag{2.40}$$

$$K_0 = \tfrac{16}{15}s_m^2 a, \quad K_2 = \tfrac{16}{105}s_m^2 a^3, \tag{2.41), (2.42}$$

$$\frac{N_a}{\alpha_2\rho} = K_1 = 2\int_0^a s^2\xi\,d\xi = \tfrac{1}{3}s_m^2 a^2 \tag{2.43}$$

from (2.21b), (2.28), (2.17) and (2.27). Note that

$$M_b = \sigma M_a = \alpha_1\rho K_0, \quad I_b = \sigma I_a = \alpha_1\rho K_2.$$

3. Recoil motions

An oscillatory lateral force of amplitude F_0 and radian frequency ω is assumed to act on the inflexible anterior part of the fish body. We write this in the complex form $F_0 e^{i\omega t}$ on the usual understanding that the real part is to be taken. The force driving the caudal fin is equal and opposite to this oscillatory reactive force. The mean longitudinal motion of the centre of mass is here assumed to be rectilinear and in the $-X$ direction. As was assumed in the previous section, the deviation $\theta-\phi$ of the body axis from the direction of motion of the centre of mass is small, and the lateral recoil movement in response to the fluctuating side forces of small amplitude is investigated here with only the lowest-order terms retained in the equations. We may put

$$V_{0X} = -U_0 \quad \text{(constant)}.$$

This suggests, as may be seen from (2.33), that the mean tangential drag $\overline{D_t^*}$ is assumed to balance the mean forward thrust $-\overline{F_t}$ generated by the caudal fin, where the overbar denotes the mean with respect to time.

Thus the governing equations are the remaining two equations (2.32) and (2.36), after substitution of (2.31) and (2.37):

$$M_0 A_{0n} = -M_a U_0\dot{\theta} - \epsilon\Phi + D_n^* + F_n, \tag{3.1}$$

$$I_0\ddot{\theta} = M_a U_0 V_{0n} - \epsilon\Psi + Q^* + F_n a, \tag{3.2}$$

where

$$F_n = F_0 e^{i\omega t}, \tag{3.3}$$

acting at $\xi = a$. In a system controlled purely by inertia ($D_n^* = Q^* = 0$) without flow ($U_0 = 0$), which leads to $\Phi = \Psi = 0$ and $A_{0n} = \dot{V}_{0n}$, it may readily be shown from (3.1) and (3.2) that these equations would make the displacement velocity

$$V_n(a) \quad (= V_{0n} + a\dot{\theta})$$

of the point $\xi = a$ lag in phase behind the force F_n by $\frac{1}{2}\pi$, or equivalently, the displacement $Y(a)$ would be in anti-phase with F_n. Such a purely reactive response would correspond to a zero average rate of working by the force. Our interest is in the modifications to this purely reactive response that result from the flow U_0, the vortex sheets shed from trailing edges (Φ and Ψ) and the resistance D_n.

Our system is controlled mainly by inertia, so that the anterior part of the fish body responds primarily to the lowest harmonic of the periodic force. Thus we may assume the simple harmonic form

$$V_n = v(\xi) e^{i\omega t}, \tag{3.4}$$

where V_n as well as $v(\xi)$ may be complex. With this form of V_n, a good approximation to the resistive force D_n given by (2.11a) is found to be

$$-\tfrac{1}{2}\rho k C_n s |v| V_n. \tag{3.5}$$

Following Lighthill (1977), we take $k = 8/(3\pi)\,(\approx 0{\cdot}849)$, which makes the expression (3.5) differ from the exact resistive force (2.11a) by only higher harmonics

$$(2n+1)\,\omega \quad (n = 1, 2, \ldots)$$

of relatively small amplitude. With respect to oscillations at the fundamental frequency, the resistance law behaves effectively as a linear resistance with damping constant $\frac{1}{2}\rho\, k C_n s |v|$.

A rigid model of the anterior part of the fish responds by means of a linear yawing motion

$$v(\xi) = v_0(1 + \xi/b), \tag{3.6}$$

where $b \equiv b_r + ib_i$ is a complex number such that $-b_r$ represents the yawing axis of the oscillatory velocity V_n.

Using the approximation (3.5) for D_n and substituting (3.4) and (3.6), we have the following expression:

$$D_n^* = \int_{-a}^{a} D_n d\xi = -Ep e^{i\omega t}, \tag{3.7}$$

where

$$p = \int_{-a}^{a} s(\xi)\,|b+\xi|\,(b+\xi)\,d\xi, \tag{3.8}$$

$$E = \tfrac{1}{2}\rho C_n k \left|\frac{v_0}{b}\right| \frac{v_0}{b}. \tag{3.9}$$

Similarly we obtain

$$Q^* = \int_{-a}^{a} D_n \xi\, d\xi = -Eq e^{i\omega t}, \tag{3.10}$$

where

$$q = \int_{-a}^{a} \xi s(\xi)\,|b+\xi|\,(b+\xi)\,d\xi. \tag{3.11}$$

Since θ is assumed small, we make the approximation $\sin\theta = \theta$ and $\cos\theta = 1$, which yields the relations

$$V_{0n} = -\dot{X}_0 \sin\theta + \dot{Y}_0 \cos\theta = \dot{Y}_0 + U_0\theta, \tag{3.12a}$$

$$A_{0n} = -\ddot{X}_0 \sin\theta + \ddot{Y}_0 \cos\theta = \ddot{Y}_0 \tag{3.12b}$$

from (2.1b), (2.3c) and (2.4 c), and also the relations

$$\dot{Y} = \dot{Y}_0 + \xi\dot{\theta}\cos\theta = \dot{Y}_0 + \xi\dot{\theta}, \tag{3.13a}$$

$$V_n = V_{0n} + \xi\dot{\theta} = \dot{Y} + U_0\theta \tag{3.13b}$$

from (2.3a), (2.6) and (3.12a). Equations (3.4) and (3.6) give

$$V_n = v_0(1 + \xi/b)\, e^{i\omega t}, \quad V_{0n} = v_0 e^{i\omega t}. \tag{3.14a, b}$$

Comparison of the coefficient of ξ in the two equivalent expressions for V_n, i.e. (3.13b) and (3.14a), gives

$$\dot{\theta} = (v_0/b)\, e^{i\omega t}. \tag{3.15}$$

Integrating this and using (3.13b), we obtain

$$\dot{Y} = V_n - U_0\theta = v_0\left(1 + \frac{\xi}{b} + \frac{iU_0}{\omega b}\right) e^{i\omega t} \tag{3.16a}$$

$$= W(\xi)\, e^{i\omega t}. \tag{3.16b}$$

Accordingly we have from (3.12b) and (3.16)

$$A_{0n} = \ddot{Y}(\xi = 0) = i\omega W_0 e^{i\omega t}, \quad W_0 = v_0(1 + iU_0/\omega b). \tag{3.17a, b}$$

Likewise we may write

$$\Phi = \Phi_1 e^{i\omega t}, \quad \Psi = \Psi_1 e^{i\omega t}, \tag{3.18a, b}$$

where

$$\Phi_1 = \alpha_2 \rho U_0 v_0 s_m^2 (1 + \tfrac{8}{15} a/b), \tag{3.19a}$$

$$\Psi_1 = \alpha_2 \rho U_0 v_0 s_m^2 a(\tfrac{8}{15} + \tfrac{1}{3} a/b) \tag{3.19b}$$

from (2.39), (2.40), (3.14b) and (3.15).

Substitution of (3.3), (3.7), (3.15), (3.17a) and (3.18a) into (3.1) yields

$$M_0 i\omega W_0 = -M_a U_0 v_0/b - \epsilon\Phi_1 - Ep + F_0, \tag{3.20}$$

where the factor $e^{i\omega t}$ has been omitted from all terms. Similarly with the aid of (3.10), (3.14b), (3.15) and (3.18b), (3.2) becomes

$$I_0 i\omega\, v_0/b = M_a U_0 v_0 - \epsilon\Psi_1 - Eq + F_0 a. \tag{3.21}$$

These two basic equations (3.20) and (3.21) determine the yawing motion specified by the amplitude v_0 of the velocity at $\xi = 0$ and the complex yawing axis b.

It is convenient to introduce the following dimensionless variables:

$$\zeta_* = F_0/M_0 s_m \omega^2 \tag{3.22}$$

and

$$v_* = v_0/s_m\omega, \quad \beta = b/a. \tag{3.23a, b}$$

Here ζ_* represents the ratio of the amplitude of the applied oscillatory force $F_0 e^{i\omega t}$ to the amplitude of the force which must be applied when the mass M_0 is oscillating with amplitude equal to the body depth s_m and the same frequency ω, whereas v_* is the corresponding ratio of lateral velocities.

Equation (3.20) can be written in the form

$$v_*\left\{i-\frac{\gamma_1}{\nu}\frac{2}{\beta}+\epsilon\frac{\gamma_2}{\nu}\frac{15\beta+8}{8\beta}+\frac{15}{16}\frac{\lambda}{\alpha_0}\frac{p(b)}{s_m a^3}\frac{|v_*|}{\beta|\beta|}\right\}=\zeta_*, \tag{3.24}$$

where

$$\nu = 2a\omega/U_0, \quad \lambda = \tfrac{1}{2}kC_n. \tag{3.25a, b}$$

Similarly, elimination of F_0 between (3.20) and (3.21) yields

$$\beta-\frac{1}{7}+\frac{i2}{\nu}(\gamma_1-\gamma_2\beta)-\epsilon\frac{i\gamma_2}{\nu}\frac{7\beta+3}{8}+i\frac{15}{16}\frac{\lambda}{\alpha_0}\frac{q(b)-ap(b)}{s_m a^4}\frac{|v_*|}{|\beta|}=0, \tag{3.26}$$

which represents the angular momentum equation about $\xi = a$. It is easy to see from (3.8) and (3.11) that we may write $p(b)/s_m a^3 = p_1(\beta)$ and $q(b)/s_m a^4 = q_1(\beta)$, where p_1 and q_1 are dimensionless functions of β. The third terms, involving the factor ϵ, in both (3.24) and (3.26) represent the contributions of the vortex sheets shed into the wake, while the fourth terms containing the factor λ represent the effect of resistance, and the second terms give the modifications due to the longitudinal motion of the body through the water. It is readily found that the solutions of (3.24) and (3.26) may be written in the form

$$\lambda v_* = f_1(\lambda\zeta_*, \nu, \gamma_1), \quad \beta = f_2(\lambda\zeta_*, \nu, \gamma_1). \tag{3.27a, b}$$

When $\zeta_* \ll 1$ and $\lambda = 8/(3\pi)$ with $C_n = 2$, solutions in the form of series expansions with respect to ζ_* may be found from (3.24) and (3.26): to lowest order

$$v_* = \zeta_*\Big/\left[i-\frac{2\gamma_1}{\beta\nu}+\epsilon_1\frac{\gamma_2}{\nu}\frac{15\beta+8}{8\beta}\right]+O(\lambda\zeta_*^2), \tag{3.28a}$$

$$\beta = \frac{1}{7}\left[1-i\frac{7}{\nu}(2\gamma_1-\epsilon_1\tfrac{3}{8}\gamma_2)\right]\Big/\left[1-\frac{i}{\nu}(2+\epsilon_1\tfrac{7}{8})\gamma_2\right]+O(\lambda\zeta_*). \tag{3.28b}$$

These show that when the frequency parameter ν is large $\mathrm{Re}\, v_* = O(\nu^{-1}\zeta_*)$ and $\mathrm{Im}\, v_* = O(\zeta_*)$, where Re and Im stand for the real and imaginary parts respectively. According to observations, the parameter ν takes values of around ten (Lighthill 1969). When ν becomes infinite in the above solution, v_* tends to $-i\zeta_*$ and β to $\frac{1}{7}$. These, however, represent an exact solution of (3.24) and (3.26) when $\nu = \infty$ and $\lambda = 0$, i.e. when the effects of both the longitudinal motion through the water and the resistance to the lateral yawing oscillations are neglected, and express the purely inertial response of $v(\xi)e^{i\omega t}$ with the yawing axis at $\xi_m = -\frac{1}{7}a$ and a phase lag of behind the force $F_0 e^{i\omega t}$, as mentioned before.

The average rate of working $\bar{E}$ by the force $F_0 e^{i\omega t}$ is given by

$$\begin{aligned}\bar{E} &= \overline{\mathrm{Re}\,[F_0 e^{i\omega t}]\,\mathrm{Re}\,[W(a)\,e^{i\omega t}]} \\ &= \tfrac{1}{2}\omega s_m F_0\,\mathrm{Re}\,[W_*] = \tfrac{1}{2}\omega s_m F_0\,\mathrm{Re}\left[v_*\left(1+\frac{1}{\beta}+i\frac{2}{\nu\beta}\right)\right],\end{aligned} \tag{3.29}$$

where

$$W_* = \frac{W(a)}{s_m\omega} = v_*\left(1+\frac{1}{\beta}+i\frac{2}{\nu\beta}\right) \tag{3.30}$$

and the relation $\overline{\mathrm{Re}\,[a_1 e^{i\omega t}]\,\mathrm{Re}\,[b_1 e^{i\omega t}]} = \frac{1}{2}\mathrm{Re}\,[\tilde{a}_1 b_1]$ has been used for the time average ($\tilde{a}_1$ = complex conjugate of a_1). This represents the work which the fish must do to overcome resistance to yawing oscillations, in addition to the work needed to produce

the lateral movements of the caudal fin in order to generate forward thrust. It is found from (3.29) and (3.28*a*, *b*) that

$$\bar{E}/\tfrac{1}{2}\omega s_m F_0 = O(\nu^{-1}\zeta_*) \quad \text{for} \quad \zeta_* \ll 1, \quad \nu \gg 1. \tag{3.31}$$

This states that the energy loss $\bar{E}$ is considerable compared with the case $\epsilon = 0$, which is considered in the next paragraph, where this considerable loss is shown to be caused by vortex shedding, although $\bar{E}$ becomes of higher order for $\nu = \infty$.

When the body sections are smoothly shaped and do not shed any vortices one may take $\epsilon = 0$. In this case one finds the following series solution for small $\lambda\zeta_*$:

$$v_* = a_1\zeta_* + a_2\lambda\zeta_*^2 + O(\lambda^2\zeta_*^3), \tag{3.32a}$$

$$\beta = \beta_0 + \beta_1\lambda\zeta_* + O(\lambda^2\zeta_*^2), \tag{3.32b}$$

where

$$a_1 = \frac{-i}{1+i2\gamma_1/\nu\beta_0}, \quad a_2 = -a_1^2|a_1|\left[P_1(\beta_0) + \frac{2\gamma_1 Q_1(\beta_0)}{(2\gamma_2+i\nu)\beta_0}\right], \tag{3.33a, b}$$

$$\beta_0 = \frac{1}{7}\frac{1-i14\gamma_1/\nu}{1-i2\gamma_2/\nu}, \quad \beta_1 = -i|a_1|Q_1(\beta_0)\Big/\left(1-i\frac{2\gamma_2}{\nu}\right), \tag{3.34a, b}$$

$$P_1(\beta_0) = \frac{15}{16}\frac{p_1(\beta_0)}{\alpha_0\beta_0|\beta_0|}, \quad Q_1(\beta_0) = \frac{15}{16}\frac{q_1(\beta_0)-p_1(\beta_0)}{\alpha_0|\beta_0|}. \tag{3.35a, b}$$

Only the first terms $a_1\zeta_*$ and β_0 are independent of λ, which represents the effect of the resistance. From (3.32*a*, *b*) and (3.29), the energy loss is

$$\begin{aligned}\frac{\bar{E}}{\tfrac{1}{2}\omega s_m F_0} &= \zeta_* \operatorname{Re}\left[-i\frac{8\nu^2+28\gamma_2}{\nu^2+28\gamma_1\gamma_2}\right] + \lambda\zeta_*^2 \operatorname{Re}\left[a_2 + \left(1+\frac{2i}{\nu}\right)\frac{\beta_0 a_2 - \beta_1 a_1}{\beta_0}\right] + O(\lambda^2\zeta_*^3) \\ &= \lambda\zeta_*^2\left\{P_1(\beta_\infty) + \frac{P_1(\beta_\infty)}{\beta_\infty} + \frac{Q_1(\beta_\infty)}{\beta_\infty^2}\right\} + O(\nu^{-1}\lambda\zeta_*^2, \lambda^2\zeta_*^2),\end{aligned} \tag{3.36}$$

where $\beta_\infty = \beta_0(\nu = \infty) = \frac{1}{7}$; note that $P_1(\beta_\infty)$ and $Q_1(\beta_\infty)$ become real in this case. It is straightforward to show that $P_1 + P_1/\beta + Q_1/\beta^2$ is $63{\cdot}504/\alpha_0$ (> 0) at $\beta = \beta_\infty$ since $p_1(\beta_\infty) = \beta_\infty + \frac{2}{3}\beta_\infty^3 - \frac{1}{15}\beta_\infty^5 = 0{\cdot}1448$ and $q_1(\beta_\infty) = \frac{1}{6} + \frac{1}{2}\beta_\infty^2 - \frac{1}{8}\beta_\infty^4 + \frac{1}{30}\beta_\infty^6 = 0{\cdot}1768$. It is remarkable that the first term of $\bar{E}$, which is proportional to ζ_*, disappears and that its leading term becomes proportional to $\lambda\zeta_*^2$; further, $\bar{E}$ vanishes when $\lambda = 0$. Thus the $\bar{E}$ in (3.36) represents only the resistive dissipation. Thus (3.31) and (3.36) suggest that the reactive effect of vortex shedding could cause an increased energy loss. This loss is proportional to $\nu^{-1}\zeta_*$ for a finite but large ν, while for small ζ_* the resistive energy dissipation is proportional to $\lambda\zeta_*^2$, which is of higher order with respect to ζ_*.

It may be of interest to define the point of action ξ_v of the vortex-sheet force by the equation

$$\xi_v = \overline{\operatorname{Re}\Psi/\operatorname{Re}\Phi}. \tag{3.37}$$

Using (3.18) and (3.19) we find

$$\xi_v = a\operatorname{Re}[5+8\beta]/\operatorname{Re}[8+15\beta] \approx 0{\cdot}61a. \tag{3.38}$$

Numerical results and discussion

A numerical method is adopted to solve the system of equations (3.24) and (3.26) for moderate ζ_*. A method of successive approximation is employed. For given values of the parameters ζ_*, ν and σ, the zeroth approximation $(v_*^{(0)}, \beta^{(0)})$ to (v_*, β) is given by

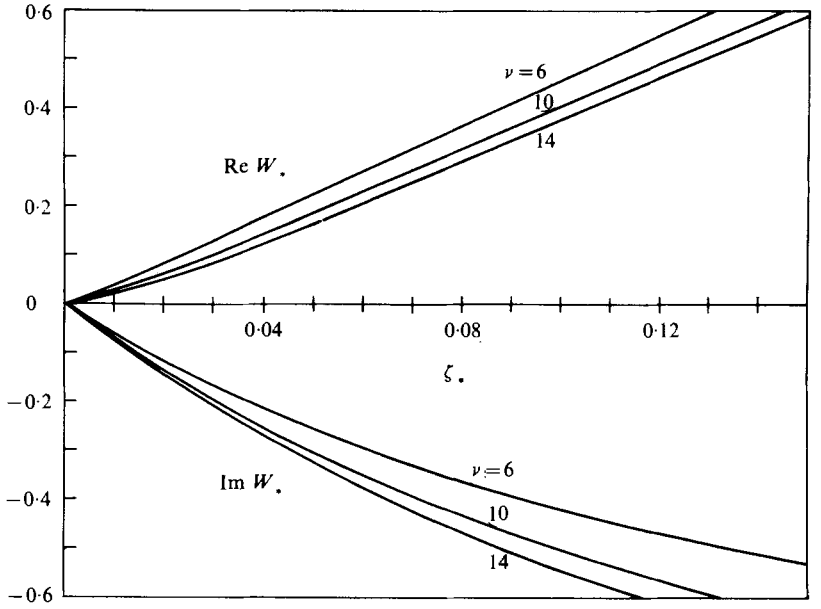

FIGURE 2. Case A ($\epsilon = 1$, $\sigma = 0{\cdot}6$): the real and imaginary parts of W_* are plotted as functions of ζ_* for various values of the reduced frequency ν; $\lambda = 8/3\pi$.

(3.28a, b). In practice, however, a known solution pair (v_*, β') for a certain ζ_*' is used as the zeroth approximation for a neighbouring ζ_*; this ensures rapid convergence. If the nth approximation $(v_*^{(n)}, \beta^{(n)})$ for a fixed ζ_* is known, the next approximation $\beta^{(n+1)}$ is sought by applying Newton's method to (3.26) with $v_*^{(n)}$ substituted in $|v_*|$. To estimate the integrals p and q defined in (3.8) and (3.11) as functions of β (or b), the factor $|\xi + b|$ is replaced by $\xi + b$ when $\xi > -\mathrm{Re}\, b$ and by $-(\xi + b)$ when $\xi < -\mathrm{Re}\, b$, since $\mathrm{Im}\, b$ is very small, as is confirmed by the final result. The $(n+1)$th approximation $v_*^{(n+1)}$ is obtained simply by substituting $\beta^{(n+1)}$ and $v_*^{(n)}$ into the curly bracket on the left-hand side of (3.24). The convergence condition is that the differences between successive values of $v_*^{(n)}$ and $\beta^{(n)}$ are both less than 10^{-5}. In this computation we always took $\lambda = 8/3\pi$ and $C_n = 2$.

The average rate of working $\bar{E}$ by the force $F_0 e^{i\omega t}$ is given by (3.29) and is proportional to $\mathrm{Re}\, W_*$. Figure 2 shows $\mathrm{Re}\, W_*$ and $\mathrm{Im}\, W_*$ *vs.* ζ_* for three values of the frequency parameter, $\nu = 6$, 10 and 14, for case A with $\sigma = 0{\cdot}6$. The imaginary part $\mathrm{Im}\, W_*$ is always negative, while the real part $\mathrm{Re}\, W_*$ is always positive, generating energy dissipation. The calculated values of $10\beta_m [= 5(1-\beta)]$ are given in table 1 for $\sigma = 0{\cdot}2$, $0{\cdot}6$ and $1{\cdot}0$. Taking account of the linear behaviour of $\mathrm{Re}\, W_*$ for small ζ_* in figure 2, as suggested by (3.28a, b), we may write $W_* = \kappa\zeta_*$ ($\kappa = \kappa_r + i\kappa_i$); then the rate of energy loss (3.29) can be written, using (3.22), as

$$\bar{E} = \tfrac{1}{2} s_m \omega F_0 \kappa_r \zeta_* = \frac{\kappa_r}{2} \frac{F_0^2}{(M_b + M_a)\omega}. \tag{3.39}$$

This suggests, with the help of the relation $M_b/\sigma = M_a \propto s_m^2 a$, that a fish whose maximum depth s_m is large enough may have a very much reduced rate of energy dissipation and also that reduction of the energy loss should be expected for a larger a. The

	$\sigma = 0{\cdot}2$	$\sigma = 0{\cdot}6$			$\sigma = 1{\cdot}0$
ζ_*	$\nu = 10$	$\nu = 6$	$\nu = 10$	$\nu = 14$	$\nu = 10$
0	$4{\cdot}32 - 0{\cdot}15i$	$4{\cdot}23 + 0{\cdot}20i$	$4{\cdot}26 + 0{\cdot}13i$	$4{\cdot}27 + 0{\cdot}09i$	$4{\cdot}24 + 0{\cdot}30i$
0·05	$4{\cdot}34 - 0{\cdot}09i$	$4{\cdot}18 + 0{\cdot}20i$	$4{\cdot}23 + 0{\cdot}14i$	$4{\cdot}23 + 0{\cdot}11i$	$4{\cdot}19 + 0{\cdot}30i$
0·10	$4{\cdot}33 - 0{\cdot}06i$	$4{\cdot}15 + 0{\cdot}19i$	$4{\cdot}20 + 0{\cdot}14i$	$4{\cdot}22 + 0{\cdot}12i$	$4{\cdot}15 + 0{\cdot}30i$
0·20	$4{\cdot}31 - 0{\cdot}02i$	$4{\cdot}12 + 0{\cdot}17i$	$4{\cdot}16 + 0{\cdot}14i$	$4{\cdot}18 + 0{\cdot}12i$	$4{\cdot}09 + 0{\cdot}27i$

TABLE 1. Values of $10\beta_m$ [$\beta_m = \frac{1}{2}(1-\beta)$] in case A, corresponding to figure 2.

ν	$\sigma = 0{\cdot}2$	$\sigma = 0{\cdot}6$	$\sigma = 1{\cdot}0$
6	$5{\cdot}54 - 5{\cdot}42i$	$4{\cdot}16 - 6{\cdot}47i$	$3{\cdot}32 - 6{\cdot}89i$
10	$3{\cdot}68 - 7{\cdot}02i$	$2{\cdot}73 - 7{\cdot}38i$	$2{\cdot}19 - 7{\cdot}54i$
14	$2{\cdot}70 - 7{\cdot}50i$	$2{\cdot}01 - 7{\cdot}67i$	$1{\cdot}61 - 7{\cdot}76i$

TABLE 2. Values of κ defined by $dW_*/d\zeta_*$ at $\zeta_* = 0$ in case A, obtained from (3.30) and (3.28a, b).

calculated values of κ are listed in table 2, which shows that κ_r is reduced both for an increased σ with ν fixed and for an increased ν with σ fixed. When σ is increased with the other parameters held constant, then the body mass M_b becomes larger (M_a fixed) and κ_r is reduced, therefore one obtains a reduced $\bar{E}$ from (3.39). (Similarly an increased frequency ω yields a reduced $\bar{E}$.) We have found that almost circular transverse cross-sections with $\sigma \lesssim 1$ in the anterior part of the body yield a smaller rate of energy dissipation due to the yawing oscillations than do flat shapes, although 'transverse compression' at the posterior end of body improves propulsive efficiency, as shown by the elongated-body theory (Lighthill 1970).

For the sake of comparison, it may be interesting to examine a fish whose trailing edges are sufficiently rounded and whose body is sufficiently slender to prevent the shedding of vortex sheets from the edges. The recoil movements of a fish of this kind can be found in the present analysis simply by putting $\epsilon = 0$ (case B). This case corresponds to that studied by Lighthill (1977). The results for this case are shown in figure 3 ($\sigma = 0{\cdot}6$) and table 3. We find a considerable reduction in Re W_* compared with the corresponding cases in figure 2, which means that the energy dissipation is much less for a recoil without vortex-sheet shedding. The curve given by the first term of (3.36) is also plotted in figure 3 for $\lambda = 8/3\pi$, $\alpha_0 = \frac{1}{4}(1+\sigma)\pi$ and $\sigma = 0{\cdot}6$.

The lateral displacement of the body during the recoil motion is found by integrating (3.16a) with respect to t and taking the real part:

$$y_* = \mathrm{Re}\left[\frac{Y}{s_m}\right] = \left|\frac{v_*}{\beta}\right| \left\{ \left(\beta_r + \frac{\xi}{a}\right) \sin(\nu\tau + \mu) + \left(\beta_i + \frac{2}{\nu}\right) \cos(\nu\tau + \mu) \right\}, \tag{3.40}$$

where $\tau = U_0 t/2a$ and $\mu = \arg(v_*/\beta)$. Note that the amplitude of the displacement is largest at $\xi = a$ (the posterior end) since it is proportional to $[(\beta_r + \xi/a)^2 + (\beta_i + 2/\nu)^2]^{\frac{1}{2}}$ and $\beta_r \approx \frac{1}{7}$. The second term in the curly brackets in (3.40) describes a sideslip motion of amplitude $|\beta_i + 2/\nu|$ independent of the position ξ, while the first corresponds to a yawing oscillation about the axis $\xi = -\beta_r a$.

According to Bainbridge (1963), there is no nodal point on the body which does not move laterally, i.e. every part of the body oscillates about the mean line of progression.

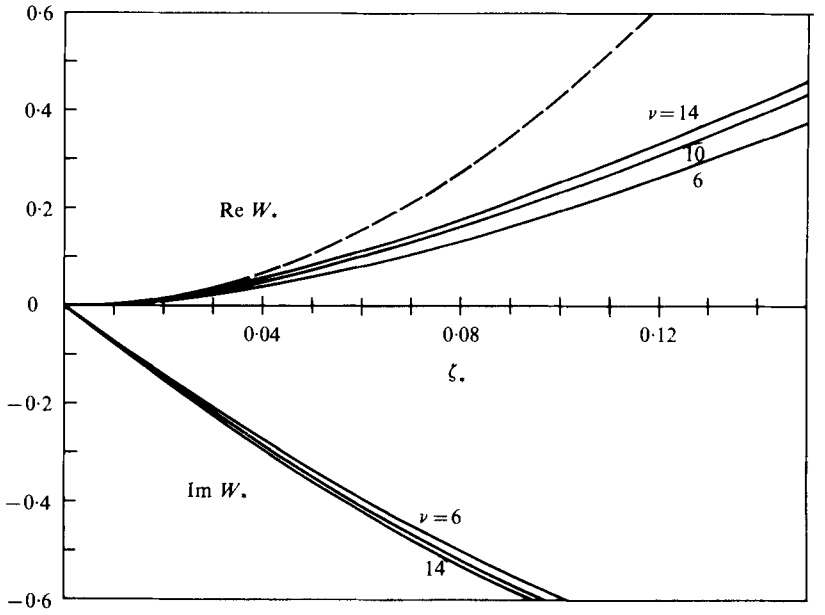

FIGURE 3. Case B ($\epsilon = 0$, $\sigma = 0{\cdot}6$): the real and imaginary parts of W_* are plotted as functions of ζ_* for various values of the reduced frequency ν; $\lambda = 8/3\pi$. The broken line is the parabolic curve given by the first term of (3.36): $(63{\cdot}50/\alpha_0)\,\lambda\zeta_*^2$.

		$\sigma = 0{\cdot}6$			
	$\sigma = 0{\cdot}2$				$\sigma = 1{\cdot}0$
ζ_*	$\nu = 10$	$\nu = 6$	$\nu = 10$	$\nu = 14$	$\nu = 10$
0	$4{\cdot}28 + 0{\cdot}05i$	$4{\cdot}19 + 0{\cdot}46i$	$4{\cdot}25 + 0{\cdot}28i$	$4{\cdot}27 + 0{\cdot}20i$	$4{\cdot}24 + 0{\cdot}42i$
0·05	$4{\cdot}25 + 0{\cdot}07i$	$4{\cdot}10 + 0{\cdot}44i$	$4{\cdot}18 + 0{\cdot}29i$	$4{\cdot}21 + 0{\cdot}22i$	$4{\cdot}17 + 0{\cdot}43i$
0·10	$4{\cdot}22 + 0{\cdot}09i$	$4{\cdot}04 + 0{\cdot}41i$	$4{\cdot}13 + 0{\cdot}28i$	$4{\cdot}17 + 0{\cdot}22i$	$4{\cdot}11 + 0{\cdot}41i$
0·20	$4{\cdot}18 + 0{\cdot}09i$	$3{\cdot}97 + 0{\cdot}35i$	$4{\cdot}07 + 0{\cdot}25i$	$4{\cdot}12 + 0{\cdot}20i$	$4{\cdot}03 + 0{\cdot}37i$

TABLE 3. Values of $10\beta_m$ [$\beta_m = \frac{1}{2}(1-\beta)$] in case B, corresponding to figure 3.

This occurs also in (3.40) if $\beta_i + 2/\nu \neq 0$, which is generally expected when ν is not infinite. The three fishes studied (dace, bream and goldfish) have a point of minimum yaw amplitude somewhere posterior to the operculum. A rough reading of Bainbridge's figures ,which give the distribution of the mean speed of lateral movement along the body length, shows that the fractional distances x_m of the point of minimum amplitude from the snout relative to the length from the snout to the anterior edge of the caudal fin are 0·36 (dace), 0·31 (bream) and 0·29 (goldfish). In the present analysis the corresponding fractional length would be defined by $\mathrm{Re}\,\beta_m$, which is 0·42 for $\epsilon = 1$ or 0 with $\zeta_* = 0{\cdot}05$, $\sigma = 0{\cdot}6$ and $\nu = 10$. According to Fierstine & Walters (1968), for the wavy-back skipjack (a scombroid fish) this point of minimum amplitude is somewhere near the base of the pectoral fin. A rough estimate of this position from their figure 1 shows that the value of x_m is around 0·31. To minimize the yawing movements at the snout, it may be preferable to have a smaller value of x_m as well as for the yawing amplitude itself to be minimized. The observed values of x_m, which are smaller than that in the

present analysis in spite of the similar lateral body shapes, may be partly due to the rather asymmetric mass distribution (more mass in the anterior half of the body of scombrids; see Fierstine & Walters) and fin arrangement.

Fierstine & Walters found for the wavyback skipjack that the snout amplitude y_0 relative to the body length is around 0·03. The corresponding expression in the present theory is

$$y_0 = \left|\frac{Y(-a)}{2a}\right| = \delta|W_*|\,\frac{|\beta-1+2i/\nu|}{|\beta+1+2i/\nu|}.$$

By using an estimated slenderness parameter $\delta \approx 0{\cdot}25$ and tables 1 and 3 ($\nu = 10$, $\sigma = 0{\cdot}6$), we obtain

$$y_0 \approx 0{\cdot}19\,|W_*|,$$

and thus

$$|W_*| \approx 0{\cdot}16 \quad \text{when} \quad y_0 = 0{\cdot}03.$$

This implies with the help of figures 2 and 3 that

$$\zeta_* \approx 0{\cdot}02 \quad \text{for both case } A \text{ and case } B.$$

At this value of ζ_* the associated energy dissipation (or equivalently $\mathrm{Re}\,W_*$) is found to remain much smaller in case B ($\epsilon = 0$) than in case A. This seems to give a clue to the reason for the folding of dorsal fins during steady swimming often observed.

4. Turning manoeuvres

According to Weihs (1972), the turning process is made up of three distinct phases characterized by different types of movement of the centre of mass. In the first stage the centre of mass continues in a straight line. A substantial turn of the nose to the side of the turn (say, left) produces lateral forces, which are to be represented in (2.30) by the **n**-component forces except for **F** (probably the main contribution is from the resistive force D_n^*). These lateral forces are almost balanced by the more effective momentum-shedding force from the caudal fin generated by a smaller movement of tail to the left [which produces a reaction force to the right, which would be represented by **F** in (2.30)]. Thus the net effect is a couple permitting rotation about the centre of mass. In the second stage the centre of mass describes a highly curved path, indicating a substantial force towards the centre of the turn, while in the last stage the centre of mass again moves in a straight line, this time in the new direction of movement. The tail becomes straight, perhaps contributing a force to balance any loss of momentum due to the drag during the turn, and finally the rotational movement of the body about the centre of mass ceases.

In our mathematical model of a turning fish, the first stage is replaced by application of an impulsive side force $F_0\mathbf{n}\,\delta(t)$ at the end $\xi = a$ to produce rotation of the body in addition to the rectilinear motion of the centre of mass. Here the subsequent turning motions of the body, corresponding to the second and third stages just described, are studied by integrating the equations of motion (2.35) and (2.36). The start of the third stage may be represented by application of another impulsive force $\mathbf{F}_1(t)$. These forces represent the shedding two vortex rings during the turn, as inferred from the work of McCutchen mentioned in § 1. It seems that the shedding of the first vortex ring contributes to the production of rotation of the body, while the shedding of the second primarily contributes to the recovery of the kinetic energy lost during the turn,

or the maintainance of the tangential velocity against drag during the turn and partly to the generation of a normal force. This is supported by the fact, shown later, that the rectilinear motion of a fish-like body is changed smoothly to a new direction by the first impulsive lateral force without requiring any counter-rotating moment generated by additional external forces, although a certain loss of kinetic energy is involved in the process. Only the effect of the first vortex ring is studied here.

Equations (2.35) and (2.36) are taken as the governing equations for the turn. Using (2.39) and (2.40), the terms H and R defined in (2.31) and (2.37) are rewritten as

$$H = -(1+\tfrac{1}{2}\epsilon)\, M_a U\dot{\theta} - \epsilon m_a(0)\, UV_{0n} - \tfrac{1}{2}\rho C_n |\dot{\theta}|\dot{\theta} P(b), \tag{4.1}$$

$$R = -\epsilon N_a U\dot{\theta} + (1-\tfrac{1}{2}\epsilon)\, M_a UV_{0n} - \tfrac{1}{2}\rho C_n |\dot{\theta}|\dot{\theta} Q(b), \tag{4.2}$$

where

$$P(b) = \int_{-a}^{a} s|b+\xi|(b+\xi)\, d\xi, \tag{4.3}$$

$$Q(b) = \int_{-a}^{a} \xi s|b+\xi|(b+\xi)\, d\xi. \tag{4.4}$$

The last terms in H and R are obtained by substituting the last expression in (2.6) into (2.23a) and (2.29), respectively.

For convenience, we non-dimensionalize (2.35) and (2.36) by dividing lengths, times, velocities, accelerations and forces by a, a/U_0, U_0, U_0^2/a and $\rho a^2 U_0^2$ respectively, where U_0 is the velocity of the rectilinear motion before application of the impulsive forces, and also dividing K_0, K_2 and masses by a^3, a^5 and ρa^3. If we substitute

$$h = H/\rho K_0, \quad \mathbf{f} = \mathbf{F}/\rho K_0, \quad d_t = D_t^*/\rho K_0, \tag{4.5a, b, c}$$

which are all divided reduced by U_0^2/a, and

$$r = R/\rho K_2, \quad c_0 = K_0/K_2, \tag{4.6a, b}$$

which are divided by $U_0^2 a^{-2}$ and a^{-2} respectively, and use the same symbols for the non-dimensional variables, then (2.35) and (2.36) read

$$\mathbf{A}_0 = (\ddot{X}_0, \ddot{Y}_0) = \alpha_0^{-1}(h+f_n)\,\mathbf{n} + \alpha_1^{-1}(d_t+f_t)\,\mathbf{t}, \tag{4.7a}$$

$$\ddot{\theta} = \alpha_0^{-1} r + \alpha_0^{-1} c_0 f_n, \tag{4.7b}$$

where

$$h = -\alpha_2 U(c_1\dot{\theta} + c_2 V_{0n}) - \tfrac{1}{2}c_5 C_n \dot{\theta}|\dot{\theta}| p(b), \tag{4.8}$$

$$r = -\alpha_2 U(c_3\dot{\theta} - c_4 V_{0n}) - \tfrac{1}{2}c_6 C_n \dot{\theta}|\dot{\theta}|\, q(b), \tag{4.9}$$

$$(c_i; i = 0, 1, \ldots, 6) = (7, 1+\tfrac{1}{2}\epsilon, \tfrac{15}{16}\epsilon, \tfrac{35}{16}\epsilon, 7(1-\tfrac{1}{2}\epsilon), \tfrac{15}{16}, \tfrac{105}{16}), \tag{4.10}$$

$$p(b) = \frac{1}{s_m}\int_{-1}^{1} (1-\xi^2)(\xi+b)|\xi+b|\, d\xi = s_m^{-1}(b + \tfrac{2}{3}b^3 - \tfrac{1}{15}b^5), \tag{4.11}$$

$$q(b) = \frac{1}{s_m}\int_{-1}^{1} \xi(1-\xi^2)(\xi+b)|\xi+b|\, d\xi = s_m^{-1}(\tfrac{1}{6} + \tfrac{1}{2}b^2 - \tfrac{1}{6}b^4 + \tfrac{1}{30}b^6) \tag{4.12}$$

and s_m, divided by a, represents twice the slenderness parameter δ.

For simplicity we assume $d_t = 0$ in the following unless specified otherwise. This is justified if the time scale of the turn is much smaller than the time scale of the deceleration due to the tangential friction drag. It is easy to show that (4.7a, b) permit

a permanent uniform motion given by $V_{0n} = 0$ and $\dot{\theta} = 0$, i.e. $\mathbf{V}_0$ and θ are constant and $\mathbf{V}_0$ is parallel to $\mathbf{t}$ provided that $\mathbf{f} = 0$. Without loss of generality, we may take the motion before the perturbation to be uniform and given by

$$X_0 = -t, \quad Y_0 = \theta = 0 \quad (t < 0). \tag{4.13}$$

We assume a perturbation in the form of the delta-function

$$\mathbf{f} = \alpha_0 I_0 \delta(t)\, \mathbf{n}, \tag{4.14}$$

which is applied at $\xi = 1$. Hence we obtain the following initial conditions by integrating (4.7a, b) with respect to t over an infinitesimal interval including $t = 0$:

$$\dot{X}_0(+0) = -1, \quad X_0(0) = 0, \tag{4.15a}$$

$$[\dot{Y}_0]_{-0}^{+0} = \dot{Y}_0(+0) = I_0, \quad Y_0(0) = 0, \tag{4.15b}$$

$$[\dot{\theta}]_{-0}^{+0} = \dot{\theta}(+0) = c_0 I_0, \quad \theta(0) = 0, \tag{4.15c}$$

where $[g]_{-0}^{+0} = \lim_{\epsilon \to +0} [g]_{-\epsilon}^{+\epsilon}$. Under these six initial conditions, the three second-order simultaneous equations (4.7a, b) can be integrated with $\mathbf{f} = 0$ for subsequent times. The total momentum change ΔP given by the impulse (4.14) is found by integrating F_n and noting the dimensionless relation $F_n = K_0 f_n = F_0 \delta(t)$, say, which gives

$$F_0 = \alpha_0 K_0 I_0.$$

Thus

$$\Delta P = \lim_{\epsilon \to 0} \int_{-\epsilon}^{\epsilon} F_n dt = F_0 = M_0 I_0, \quad \text{where} \quad M_0 = \alpha_0 K_0, \tag{4.16a, b}$$

this dimensionless form (4.16b) being obtained from (2.34). In dimensional form, we have

$$\Delta P = M_0 U_0 I_0, \tag{4.17}$$

from which we readily see the meaning of the intensity factor I_0 in the disturbance (4.14). Using (2.34) and (2.41), one readily obtains $\Delta P / \alpha_0 \rho a U_0 = \frac{16}{15} s_m^2 I_0$.

Small perturbations

Investigation of infinitesimal perturbations to the uniform rectilinear motion (4.13) of a fish-like body not only helps in deciding whether or not the motion is dynamically stable, but also supplies the asymptotic behaviour in the final period of a turn. Moreover it leads to a full description of the motion that follows a given initial perturbation. In the preceding section we considered uniform motion characterized by $V_{0n} = \dot{\theta} = 0$. In a perturbed motion V_{0n} and $\dot{\theta}$ are taken as small quantities (θ is not necessarily small) and therefore the drag terms proportional to $\dot{\theta}|\dot{\theta}|$ in the definitions (4.8) and (4.9) of h and r are neglected here. The governing equations take the same form as (4.7a, b) except that

$$h = -\alpha_2 U(c_1 \dot{\theta} + c_2 V_{0n}), \tag{4.18a}$$

$$r = -\alpha_2 U(c_3 \dot{\theta} - c_4 V_{0n}). \tag{4.18b}$$

These are equivalent to the equations of motion in a dragless fluid. Introducing a unit vector $\mathbf{e} \equiv (-\cos\phi, -\sin\phi)$, we can write $\mathbf{V}_0 = V_0 \mathbf{e}$, where V_0 is the magnitude of

the velocity of the centre of mass, ϕ being defined in (2.5). Then one has

$$\mathbf{A}_0 = \dot{V}_0\mathbf{e} + V_0\dot{\mathbf{e}} \approx -\dot{V}_0\mathbf{t} - V_0\dot{\phi}\mathbf{n}, \tag{4.19a}$$

$$U = -\mathbf{V}_0 . \mathbf{t} = V_0 \cos(\theta - \phi) \approx V_0, \tag{4.19b}$$

$$V_{0n} = \mathbf{V}_0 . \mathbf{n} = V_0 \sin(\theta - \phi) \approx V_0(\theta - \phi), \tag{4.19c}$$

where V_0 and $\theta - \phi$ are taken as small and therefore $\mathbf{e}$ and $\dot{\mathbf{e}}$ are replaced in (4.19a) by $-\mathbf{t}$ and $-\dot{\phi}\mathbf{n}$ respectively. Substitution of (4.19a) into (4.7a) yields

$$-\alpha_1\dot{V}_0 = f_t, \quad -\alpha_0 V_0\dot{\phi} = h + f_n. \tag{4.20), (4.21}$$

From (4.20), we have $V_0 =$ constant when $f_t = 0$ [or when $f_t + d_t = 0$ in (4.7a)]. We assume f_n to be of the form (4.14). Thus using (4.18a, b) and (4.19c), (4.21) and (4.7b) can be written as

$$\dot{\phi} = \gamma_2[c_1\dot{\theta} + c_2 V_0(\theta - \phi)] - (I_0/V_0)\,\delta(t), \tag{4.22}$$

$$\ddot{\theta} = -\gamma_2 V_0[c_3\dot{\theta} - c_4 V_0(\theta - \phi)] + c_0 I_0\delta(t), \tag{4.23}$$

where $\gamma_2 = 1/(1+\sigma)$. Elimination of $\theta - \phi$ between these equations leads to

$$c_2\ddot{\theta} = -\gamma_2 V_0(c_2c_3 + c_1c_4)\,\dot{\theta} + c_4 V_0\dot{\phi} + (c_2c_0 + c_4)\,I_0\delta(t). \tag{4.24}$$

Equations (4.22) and (4.24) constitute a pair of differential equations for ϕ and θ with a disturbing impulse given by a δ-function. To integrate, one makes the assumption

$$\phi = C + Ae^{\lambda t}, \quad \theta = C + Be^{\lambda t} \quad (t > 0), \tag{4.25a, b}$$

where C is a constant common to both ϕ and θ, and the constants A and B are assumed small. According to whether $\mathrm{Re}\,\lambda$ is negative or positive, the deviation angle $\theta - \phi$ tends to zero or infinity as $t \to \infty$, and the state of motion may be called stable or unstable, respectively. Substituting (4.25a, b) into (4.22) and (4.24) supplies for $t > 0$

$$(\lambda + \gamma_2 c_2 V_0)\,A = \gamma_2(c_1\lambda + c_2 V_0)\,B, \tag{4.26a}$$

$$[c_2\lambda + \gamma_2 V_0(c_2c_3 + c_1c_4)]\,B = c_4 V_0 A. \tag{4.26b}$$

These are two linear homogeneous equations for A and B and yield non-trivial solutions only if λ satisfies the equation

$$\left(\frac{\lambda}{\gamma_2 V_0}\right)^2 + (c_2 + c_3)\frac{\lambda}{\gamma_2 V_0} + c_1c_4 + c_2c_3 - \frac{c_4}{\gamma_2} = 0, \tag{4.27}$$

whose two roots are given by

$$\lambda = \tfrac{1}{2}\gamma_2 V_0\{-(c_2 + c_3) \pm G^{\frac{1}{2}}\}, \tag{4.28}$$

where

$$G = (c_2 - c_3)^2 - 4c_1c_4 + 4c_4/\gamma_2. \tag{4.29}$$

If the two roots coincide, i.e. $G = 0$, the forms of (4.25a, b) permit only one solution with $\lambda = \lambda_1$, where $\lambda_1 = -\tfrac{1}{2}\gamma_2 V_0(c_2 + c_3)$. Another independent solution is found to be of the form

$$\phi = At\exp(\lambda_1 t), \quad \theta = Bt\exp(\lambda_1 t).$$

One finds $\lambda_1 < 0$ for the c_2 and c_3 given in (4.10) with $\epsilon = 1$. In general, using the c_i's in (4.10), one obtains from (4.28) and (4.29)

$$\lambda = \tfrac{1}{2}\gamma_2 V_0(-\tfrac{25}{8} \pm G^{\frac{1}{2}}), \quad G = 311(\tfrac{224}{311} - \gamma_2)/16\gamma_2. \tag{4.30a, b}$$

Thus for $\gamma_2 > \gamma_2^* = \frac{224}{311}$ ($\approx 0{\cdot}72$), (4.27) has two complex-conjugate roots with negative real parts ($\gamma_2 V_0 > 0$), and therefore disturbances damp in an oscillatory manner. For $\gamma_2 < \gamma_2^*$, there are two cases: one with two negative real roots, the other with one negative and one positive real root. The critical value of γ_2 dividing the two cases, i.e. the value γ_c at which transition from stability to instability occurs, is given by

$$\gamma_c = c_4/(c_1 c_4 + c_2 c_3), \tag{4.31}$$

yielding $\gamma_c = \frac{128}{267} = 0{\cdot}4794$ ($\sigma_c = (1-\gamma_c)/\gamma_c = 1{\cdot}086$), below which (or for σ above σ_c) we find a positive real root. This result can be summarized as follows: the state of rectilinear uniform motion is unstable if $\gamma_2 < \gamma_c$, while disturbances damp monotonically for $\gamma_c < \gamma_2 \leqslant \gamma_2^*$ and damp in an oscillatory manner for $\gamma_2^* < \gamma_2 < 1$.

It may be interesting to note that the motion is always unstable if no vortex sheet is shed from the trailing (side) edge, i.e. $\epsilon = 0$. In this case one has

$$(c_1, c_2, c_3, c_4) = (1, 0, 0, 7),$$

for which (4.27) reduces to $$\frac{\lambda}{\gamma_2 V_0} = \pm \left[7\left(\frac{1}{\gamma_2} - 1\right)\right]^{\frac{1}{2}}.$$

Thus we always have one positive real root (exponentially growing solution) since $\gamma_2 < 1$. This is consistent with the well-known theorem in the theory of the motion of a rigid body without vortex shedding (irrotational flow around a solid in motion) that translational motion of an ellipsoid in the direction of its longest axis is unstable (Lamb 1932, art. 124). We may say that, although our fish-like model is not ellipsoidal, its longitudinal axis would correspond to the unstable axis of the ellipsoid.

From (4.22) and (4.24) much more information can be obtained about the behaviour of the body than merely a stability criterion. One can analyse in detail the kind of motion that sets in after a body in steady rectilinear motion with velocity V_0 has been disturbed by an impulsive force so long as $\phi - \theta$ remains small. As mentioned earlier, this may be either motion caused by a small perturbation or motion in a hypothetical dragless fluid. We may take $V_0 = 1$.

Equation (4.27) is assumed to have two different roots λ_1 and λ_2 ($\lambda_1 > \lambda_2$). Then for each of these, say λ_1, one obtains from (4.26a) or (4.26b) a ratio $\kappa_1 = B_1/A_1$ and thus the corresponding solution pair $(A_1 \exp(\lambda_1 t), \kappa_1 A_1 \exp(\lambda_1 t))$ for (ϕ, θ). The fact that (4.22) and (4.24) are linear and homogeneous for $t > 0$ leads to a general solution of the form

$$\phi = \phi_\infty + A_1 \exp(\lambda_1 t) + A_2 \exp(\lambda_2 t), \tag{4.32a}$$

$$\theta = \phi_\infty + B_1 \exp(\lambda_1 t) + B_2 \exp(\lambda_2 t), \tag{4.32b}$$

where $$B_1 = \kappa_1 A_1, \quad B_2 = \kappa_2 A_2, \tag{4.33}$$

and the three arbitrary constants ϕ_∞, A_1 and A_2 are introduced, since (4.22) is a first-order differential equation and (4.23) a second-order differential equation.

The initial conditions are obtained from (4.22) and (4.23) as before:

$$\phi(+0) = -I_0, \quad \theta(+0) = 0, \quad \dot{\theta}(+0) = c_0 I_0,$$

which become on using (4.32*a*, *b*)

$$\phi_\infty + A_1 + A_2 = -I_0, \tag{4.34a}$$

$$\phi_\infty + \kappa_1 A_1 + \kappa_2 A_2 = 0, \tag{4.34b}$$

$$\lambda_1 \kappa_1 A_1 + \lambda_2 \kappa_2 A_2 = c_0 I_0. \tag{4.34c}$$

This system of algebraic equations for ϕ_∞, A_1 and A_2 can be readily solved, yielding

$$\phi_\infty = (I_0/D)\{\kappa_1\kappa_2(\lambda_1 - \lambda_2) + c_0(\kappa_2 - \kappa_1)\}, \tag{4.35a}$$

$$A_1 = (I_0/D)\{\lambda_2\kappa_2 - c_0(\kappa_2 - 1)\}, \tag{4.35b}$$

$$A_2 = (I_0/D)\{-\lambda_1\kappa_1 + c_0(\kappa_1 - 1)\}, \tag{4.35c}$$

where $D = \kappa_1\kappa_2(\lambda_2 - \lambda_1) + \kappa_1\lambda_1 - \kappa_2\lambda_2$, the determinant of the coefficients of the system of equations (4.34*a*, *b*, *c*). As an example we take a model of elliptic cross-section with $\sigma = 0{\cdot}6$, giving $\gamma_2 = 0{\cdot}625$. The expression (4.28) with $V_0 = 1$ gives

$$\lambda_1 = -0{\cdot}4387, \quad \lambda_2 = -1{\cdot}5144, \tag{4.36}$$

then (4.26*a*, *b*) yield

$$\kappa_1 = 0{\cdot}8430, \quad \kappa_2 = 1{\cdot}1135. \tag{4.37}$$

Thus one finds from (4.33) and (4.35) that

$$(\phi_\infty, A_1, A_2, B_1, B_2) = I_0(9{\cdot}465, -8{\cdot}088, -2{\cdot}377, -6{\cdot}818, -2{\cdot}647). \tag{4.38}$$

The behaviour of the angle ϕ given by (4.32*a*) and (4.36) shows a monotonic approach to the limiting angle ϕ_∞, the final direction of motion. This angle is found to be proportional to the magnitude of the impulse I_0 from (4.38):

$$\phi_\infty = 9{\cdot}465 \quad I_0 = 9{\cdot}465\, F_0/M_0, \tag{4.39}$$

where (4.16*a*) has been used. It is found that an infinitesimal perturbation gives rise to an infinitesimal change in the direction of motion. In this sense the present system is not 'stable' in the usual sense that the original state is recovered, but may be called 'quasi-stable'. Comparison between this ϕ_∞ and the final angle obtained from the full expressions (4.7*a*, *b*), described in the next subsection, shows the effect of the normal drag D_n.

Numerical results

A numerical investigation of (4.7*a*, *b*) has been made under the initial conditions (4.15*a*, *b*, *c*) by the Adams–Bashforth method. The parameters involved are the depth parameter s_m and the shape parameter σ of the cross-section, which is fixed at a typical value 0·6. Also, the drag coefficient C_n is fixed at 2·0.

Figures 4(*a*), 4(*b*) and 6(*a*) show, respectively, the time development of θ, $\theta - \phi$ and $V_0^2(t)/V_0^2(0)$ (the kinetic energy of the body relative to the initial kinetic energy, where $V_0^2(t) = V_{0X}^2 + V_{0Y}^2$) for case *A* ($\epsilon = 1$) for $s_m = 0{\cdot}6$ and different values of η, where $\eta = (s_m/0{\cdot}2)^2 I_0 = 9I_0$ (the introduction of the factor $(s_m/0{\cdot}2)^2$ will be explained later). The broken curves in figure 4(*a*) are the analytical curves given by (4.32*b*) with (4.36) and (4.38) for $\eta = 0{\cdot}1$ and 1·0, where the normal drag term is neglected

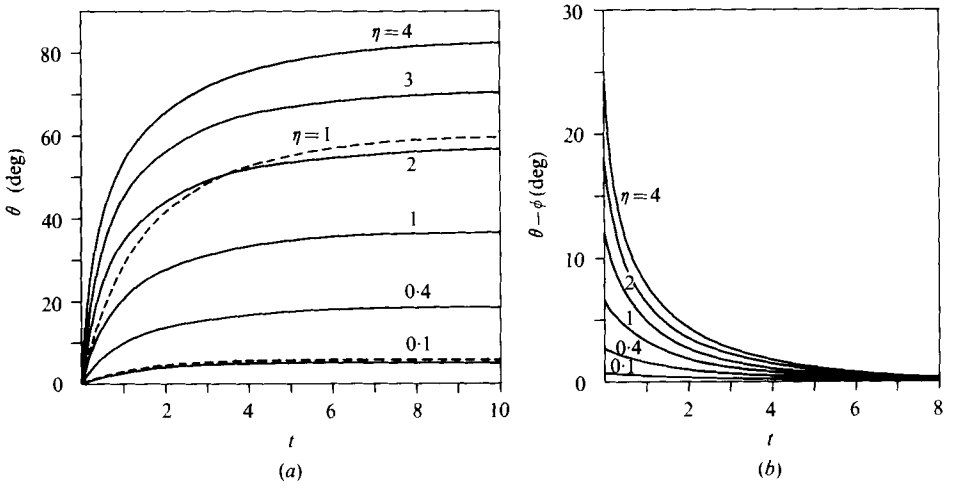

FIGURE 4. Case A ($\epsilon = 1$, $s_m = 0{\cdot}6$, $\sigma = 0{\cdot}6$, $C_n = 2$): evolution with time t of (*a*) θ and (*b*) $\theta - \phi$ for fixed η ($= 9I_0$). The broken curves show the reactive responses (without resistance) given by (4.32*b*) with (4.36) and (4.38) for $\eta = 0{\cdot}1$ and 1.

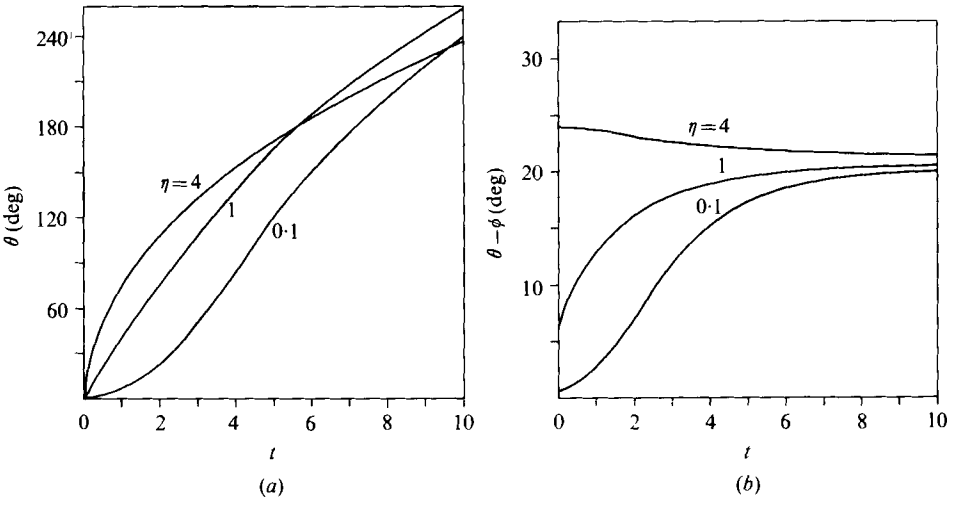

FIGURE 5. Case B ($\epsilon = 0$, $s_m = 0{\cdot}6$, $\sigma = 0{\cdot}6$, $C_n = 2$): evolution with time t of (*a*) θ and (*b*) $\theta - \phi$ for various values of η ($= 9I_0$).

as well as the tangential drag term. Thus the contribution from the normal drag is given here by the difference between the solid and broken curves with the same η and leads to a reduction in the angle of turn. The reduction is larger for larger η. One finds from these figures that both $\theta(t)$ and $V_0(t)$ tend to limiting values depending on η while the difference angle $\theta - \phi$ damps rapidly.

As shown in the small perturbation analysis, the rectilinear motion is unstable if $\epsilon = 0$ (case B), i.e. if no vortex sheet is shed from the trailing edge. For this case curves of θ, $\theta - \phi$ and $V_0^2(t)/V_0^2(0)$ *vs.* t for various η's are given in figures 5(*a*), 5(*b*) and 6(*b*), respectively, and show that θ is still increasing at $t = 10$ while V_0 is decreasing. This is in striking contrast to the corresponding behaviour when $\epsilon = 1$ given above.

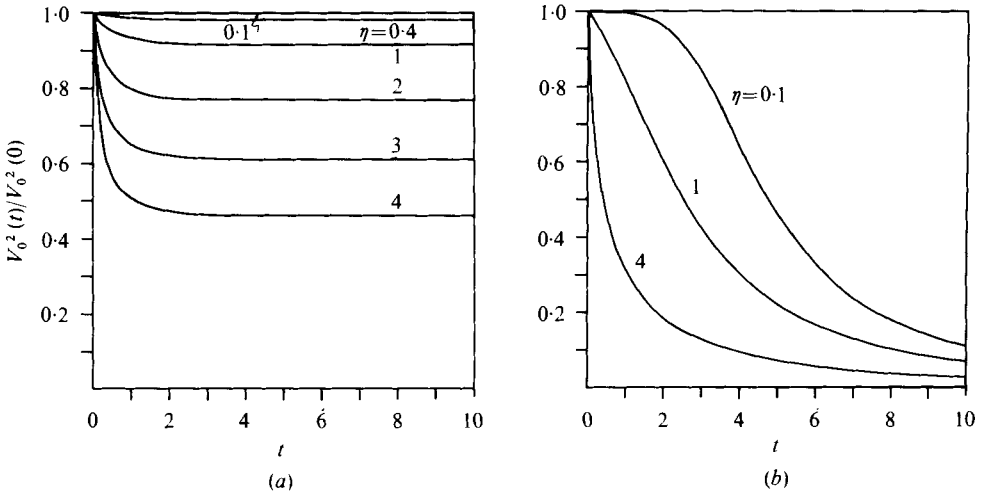

FIGURE 6. Evolution with time t of the kinetic energy of motion $\frac{1}{2}M_b V_0^2(t)$ relative to the initial kinetic energy $\frac{1}{2}M_b V_0^2(0)$ for various values of η: (*a*) case *A*, corresponding to figure 4; (*b*) case *B*, corresponding to figure 5.

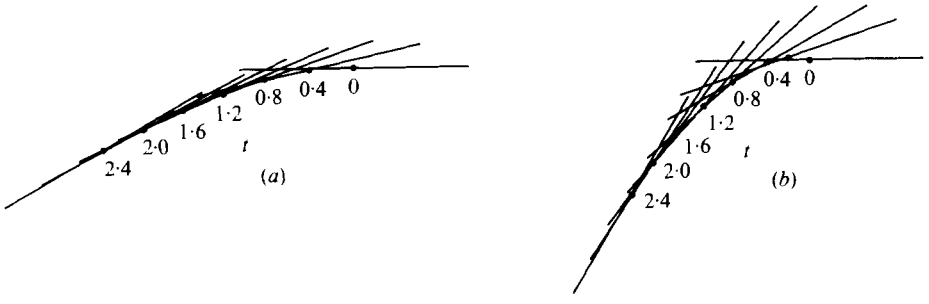

FIGURE 7. Time sequence of positions of the longitudinal body axis in case *A*, corresponding to figure 4: (*a*) $\eta = 1$; (*b*) $\eta = 3$. The dot shows the position of the centre of mass at each time marked, the time unit being a/U_0.

Another remarkable change from the previous case is found in the difference angle $\theta - \phi$, which does not tend to zero as t becomes large. Observations show that, in scombroid fishes with triangular 'sail-shaped' (Wu 1971) fins, the first dorsal fin can be completely retracted into a groove in the dorsal surface of the body (Harris 1936). Also, many teleosts are seen to erect the first dorsal fin during a turn, probably to enable the difference angle to approach zero and the body rotation to stop rapidly, while normally this fin is depressed during swimming and gliding. This reminds us of the result in § 3 that the energy loss associated with recoil movements is minimized when vortex shedding is absent.

A time sequence of positions of the longitudinal body axis is plotted in figures 7(*a*) and (*b*) for $\eta = 1$ and $\eta = 3$, respectively, with $\epsilon = 1$ and $\sigma = 0{\cdot}6$ (the time unit being a/U_0). The path of the centre of mass is to the right at first, conforming with the initial impulse, then turns to the left, as clearly shown in figure 7(*b*). Note that these diagrams are compared with tracings of the position of the backbone of a rudd during a turn in Weihs (1972).

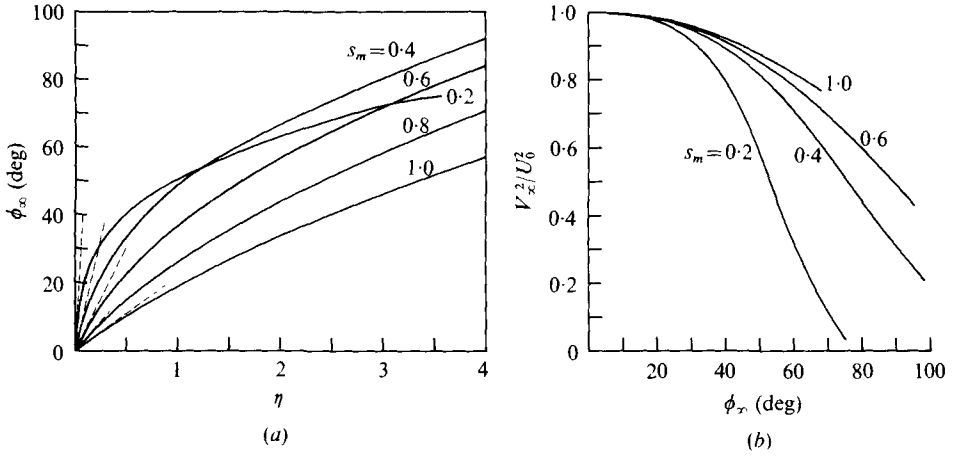

FIGURE 8. Case A ($\epsilon = 1$, $\sigma = 0{\cdot}6$, $C_n = 2$). (a) Final angle of turn ϕ_∞ *vs.* η ($= I_0(s_m/0{\cdot}2)^2$) for various values of s_m. The broken lines show the reactive response (4.39). (b) The ratio of the final kinetic energy $\frac{1}{2}M_b V_\infty^2$ to the initial kinetic energy $\frac{1}{2}M_b U_0^2$ *vs.* ϕ_∞ for fixed s_m. Note that $d_t = 0$ is assumed in the numerical computation.

The final angle of turn ϕ_∞ is plotted in figure 8 (a) against η for $\epsilon = 1$ and five values of s_m, where $\eta = I_0(s_m/0{\cdot}2)^2$, so that the total applied impulse ΔP is unchanged if η is fixed for the various s_m's as is readily seen from the statement just below (4.17). This figure tells us that for a fixed lateral impulse ΔP the angle of turn ϕ_∞ increases with decreasing s_m (or decreasing slenderness parameter δ) except for very slender fish with $s_m = 0{\cdot}2$. The broken straight lines tangential to each curve at $\eta = 0$ are those given by (4.39), which represents the reactive response of a body shedding a vortex sheet without any resistive drag. The reduction in the angle of turn due to the drag is found from the difference between these lines and the curves. Figure 8 (b) shows the ratio of the final kinetic energy $\frac{1}{2}M_b V_\infty^2$ to the initial kinetic energy $\frac{1}{2}M_b U_0^2$ for four different s_m's. Its difference from unity gives the relative energy loss during the turn. Note that in this computation the tangential drag is neglected and therefore the loss is caused by the reactive force due to the vortex sheet and the normal drag. We find from the figure that the loss is very small if the turning angle is small, or equivalently the lateral impulsive force is small. Even for a turn through 40°, the loss is as small as 10 % except for very slender fish with $s_m = 0{\cdot}2$. The figure suggests that if a large angle of turn, say 90°, is required, not a single turn but two turns through 45°, for example, may be better from the point of view of economy of energy if enough time and space are available. From figure 8 (a) one can estimate the magnitude of the impulse ΔP to be applied in the turn. For a typical fish with $s_m = 0{\cdot}5$ and $\sigma = 0{\cdot}6$, the impulse ΔP is given by $I_0 M_0 U_0 = (1 + 1/\sigma)(0{\cdot}2/s_m)^2 \eta M_b U_0 = 0{\cdot}427\eta M_b U_0$. The figure shows that $\eta \approx 1$ for $\phi_\infty = 45°$ and $\eta \approx 3{\cdot}24$ for $\phi_\infty = 80°$, corresponding to the turning of a rudd studied by Weihs (1972). Thus one finds that $\Delta P = 0{\cdot}43 M_b U_0$ for $\phi_\infty = 45°$ and $1{\cdot}39 M_b U_0$ for $\phi_\infty = 80°$.

Discussions

Two ways in which a flying object can turn are known in the theory of flight (von Mises 1945). In the banked turn used in regular cases the lift of the aeroplane, say, which is brought into an inclined position by operating the ailerons, supplies the cross-force

needed for the turn. In the so-called 'flat turn', on the other hand, the wings are kept horizontal, but the instantaneous direction of flight does not necessarily coincide with the longitudinal axis of the aeroplane, the balancing moments being provided by an appropriate setting of the control surfaces (elevators, rudder and ailerons). The deviation angle, called the sideslip, would produce the cross-component of the aerodynamic forces, called the 'side force', needed to produce the centripetal acceleration. The contributions to the side force may come mainly from the aerodynamic forces acting on the vertical control surfaces and the aeroplane body. The situation resembles closely the case of the turning of a fish in water studied here. The point to be noted is due to the difference in densities of the air and water. The small density of air (compared with the average density of the aeroplane body) makes the flat turn less important in flight. It is considered that the flat turn becomes important for directional control in water since the lift force balancing the weight of the body almost vanishes. It may be interesting to compare this motion with the motion of a solid in a vacuum which is acted on by an impulsive lateral force to the right at the rear end during its uniform motion. The subsequent motions of the centre of mass of the body would be quite different: the motion in the vacuum would be to the right, while that in water would be to the left.

The stability analysis in this section has shown that the (yawing) motion in the X, Y plane is stable if $\sigma < 1{\cdot}086$ for case A ($\epsilon = 1$). However this does not imply stability to motion in the Z direction (pitching motion). Simultaneous stabilization of both types of motion seems to be impossible, so that when the cross-sections are of the shape stable to yawing motion some additional organs will be required in order to ensure stability to pitching motions.

Harris (1936) studied the action of the fins of a typical shark in producing statically stable forward motion. He found that the yawing equilibrium of the shark is controlled almost entirely by the median fins, whose function has been considered in the present paper in the context of the ribbon-fins, while the pitching equilibrium is largely dependent on the configuration of the paired fins, and is scarcely affected by the presence or absence of the median fins.

In some fishes, e.g. scombrids, one finds another type of stabilizer whose position and function seem quite similar to those of the horizontal stabilizer of an aeroplane. This organ, called the 'keel', lies on both sides of the peduncle (point of minimum depth). The tunnyfish has a pair of fleshy keels in the horizontal plane including the longitudinal body axis, while the spearfish has two pairs of fleshy keels above and below this plane, both fishes being strong, active swimmers. Although the total area S_0 of the fleshy keel's planform is small, its stabilizing pitching moment is considered to be sufficient owing to its considerable distance l_0 from the centre of mass and the high swimming speed U_0, since the moment would be approximately proportional to $l_0 S_0 U_0^2$. A rough estimate of the ratio of the total keel area S_0 to the dorso-ventral projected area of the whole body in a tunnyfish is 0·02. Interestingly enough, the corresponding ratio of the total area of the horizontal surfaces (stabilizers) at the posterior end of a Japanese submarine (at the time of World War II; see *Plans of Ships of the Imperial Japanese Navy*, Soc. Naval Archit. Japan, 1975) to its projected area in the horizontal plane is around 0·03.

I am very grateful to Professor Sir James Lighthill for his interest in this work, and particularly his kindness in showing me his enlightening work (1977) prior to its publication and also reading the original manuscript. Assistance provided by Mr K. Shiraishi in numerical studies is greatly appreciated.

REFERENCES

BAINBRIDGE, R. 1963 *J. Exp. Biol.* **40**, 23.
CHOPRA, M. G. & KAMBE, T. 1977 *J. Fluid Mech.* **79**, 49.
FIERSTINE, H. L. & WALTERS, V. 1968 *Mem. S. Calif. Acad. Sci.* **6**, 1.
FLACHSBART, O. 1935 *Z. angew. Math. Mech.* **15**, 32.
GRAY, J. 1933 *Proc. Roy. Soc.* B **113**, 115.
GRAY, J. 1968 *Animal Locomotion.* Weidenfeld & Nicolson.
HARRIS, J. E. 1936 *J. Exp. Biol.* **13**, 476.
LAMB, H. 1932 *Hydrodynamics.* Cambridge University Press.
LIGHTHILL, M. J. 1960 *J. Fluid Mech.* **9**, 305.
LIGHTHILL, M. J. 1969 *Ann. Rev. Fluid Mech.* **1**, 413.
LIGHTHILL, M. J. 1970 *J. Fluid Mech.* **44**, 265.
LIGHTHILL, M. J. 1977 In *Fisheries Mathematics* (ed. J. H. Steele). Academic Press.
MCCUTCHEN, C. W. 1976 *J. Exp. Biol.* **65**, 11.
MISES, R. VON 1945 *Theory of Flight.* McGraw-Hill.
NEWMAN, J. N. & WU, T. Y. 1973 *J. Fluid Mech.* **57**, 673.
WATANABE, Y. & KIMURA, M. 1977 *Proc. 8th Int. Cong. Cybernetics, Ass. Int. Cybernetique, Namur, Belgium*, 1976.
WEIHS, D. 1972 *Proc. Roy. Soc.* B **182**, 59.
WU, T. Y. 1971 *J. Fluid Mech.* **46**, 545.